An analytical model for wind-driven Arctic summer sea ice drift

H.-S. Park and A. L. Stewart

Response to Anonymous Reviewer #1

We thank the reviewer for their comments on our paper. We have revised the manuscript in accordance with these comments and those of the other reviewer. In particular, we added plots showing the effect of ice concentration on ice speed as and wind-ice (& ice-ocean) velocity angles – with these plots, we added caveats in several places that our model may overestimate ice drift speed and velocity angles because the internal stress is neglected. Moreover we added a section (Sec 2.3) that discusses similarities and differences between our analytical model and Rossby similarity theory. Below we address the reviewer's comments individually.

I found the application of the model to the large scale changes observed during ice retreat in the Arctic less interesting. The hypothesis that such ice retreat can be wind driven is hardly novel and the authors do indeed provide references to earlier work on the subject.

➔ This part of the paper serves a dual purpose. First, it is a test of our model's assumptions that the summer sea ice drift can be described accurately by neglecting internal stresses and assuming constant drag coefficients at the ice-ocean, atmosphere-ice, and atmosphere-ocean interfaces. Second, by extension, it tests the hypothesis that the anomalous reduction in sea ice concentration in the Pacific sector during southerly wind events can be attributed to the mechanical effect of wind-driven ice drift, rather than thermodynamic effects. This is novel because we are able to draw a direct dynamical link, rather than a statistical one, between the southerly strengthening events and the anomalous changes in sea ice concentration. We focus on southerly wind strengthening events because they contribute significantly to the annual retreat of Arctic sea ice. Furthermore our model is most applicable in mid-summer, when the sea ice concentration is relatively low and internal stress is less dynamically important, and during periods of unusually strong winds, when the wind driven Ekman layer velocity will be unusually strong and thus our assumption of a negligible geostrophic ocean velocity will be more accurate. We have now emphasized the purpose of this part of the paper in our abstract, introduction and conclusion.

Their method appears to be applicable to a large number of such events and could possibly give

us insights into those, but the authors make little use of it. They primarily discuss one event and then show how using their model is better than using classical free drift.

➔ Though it may not have been sufficiently clear in the original text, our analysis of wind-driven ice retreat actually encompasses 27 intra-seasonal southerly wind events identified between 1990 and 2012, rather than being focused on a single event. We have attempted to make this clearer in the text of section 5.

I think it would have been worth while also to consider the results of the PIOMAS model in this comparison or better yet, satellite observations of the actual ice drift speed (although these can be lacking during this period, I'm not sure). This could give use a better indication of the quality of the model results than just comparing to the classical free drift. I'm not sure what the authors wanted to do with this application of the model, but it feels like an after thought and unfinished.

➔ Using ice drift inferred from satellite observations is certainly a possibility and a welcome suggestion from the reviewer. After some consideration, we have chosen to retain our focus on the sea ice concentration rather than the ice drift velocity. Ice drift products exhibit considerable uncertainty, particularly during summer when the ice is typically thinner (Sumata et al., 2014). There is considerable variance in the ice speed and the wind-ice velocity angle even in the ITP-V data (see Figs. 3 and 4), in which the ice velocities are measured accurately using GPS fixes. Thus a point-by-point comparison between our model predictions and the summer sea ice velocities from ice drift products would essentially be a more extensive version of the model evaluation performed in section 4 (though admittedly using data from summer) but with much more uncertainty in the ice drift velocity. More prosaically, changes in the sea ice concentration itself are of the most interest from an Arctic climate perspective, so we believe that comparisons between the modeled and observed sea ice concentration anomalies will be of broader interest to other scientists. We have now provided a brief discussion to this effect in section 5.

Specific comments:

I was a bit worried and confused by your repeated use of the $\varphi = 1$ case. You are considering the free drift approximation which breaks down in this case due to the influence of internal stresses. As such, you cannot use the $\varphi = 1$ case to do anything, unless you have thoroughly shown that the difference between $\varphi = 1$ and a lower value (say $\varphi = 0.8$) is negligible. This is indicated in figure 4, but should be done earlier and be underlined much better.

➔ As the reviewer suggests, we added plots showing our model results with 50% ice cover (φ =

0.5) in Figures 3 and 4 in the revised manuscript. With these plots, we added discussions in several places that our model may overestimate ice drift speed and wind-ice velocity angle because the internal stress is neglected. We have also modified the text of section 2 to acknowledge that the 100% sea ice concentration is inconsistent with the free drift approximation, but provides a good approximation to the general model solution to for $\varphi \geq 0.5$.

Technical corrections and minor specific comments:

Page 2102 Line 9: There's really no such thing as _surface_ geostrophic velocity -please rephrase.

➔ We have changed "ocean surface geostrophic velocity" to "ocean geostrophic velocity".

I don't like this abstract. It is not representative of what happens in the paper, putting nearly all the emphasis on the simulation of ice retreat, which in reality is only a small portion of the paper. I suggest you completely rewrite the abstract so that it is more faithful to the paper contents.

➔ We have now rewritten the abstract to more accurately reflect the contents of the article, putting more emphasis on the analytical model description and evaluation sections of the paper.

Line 24: Referencing Hibler (1979) is not appropriate in this context - it's a modeling paper, but you want to cite observations.

➔ As the reviewer suggests, we deleted the reference to Hibler (1979).

Line 25: Thorndike and Colony considered the geostrophic velocity, while Cole et al considered the ocean surface velocity. This needs to be made clearer here.

➔ Cole et al. (2014) is cited in the subsequent sentence: "On time scales from days to months, surface wind variability explain more than 70% of the sea-ice motion (Thorndike and Colony, 1982), and is well correlated with the surface ocean velocity (Cole et al., 2014).

Page 2103 Line 2: Again, referencing a modelling paper (Kawaguchi and Mitsudera, 2008) is not appropriate here.

➔ As the reviewer suggests, we deleted the reference to Kawaguchi and Mitsudera (2008).

Line 9: This paragraph is too long, addresses multiple topics, and should be split up.

➔ We have now divided this paragraph into two, one which discusses previous sea ice and boundary layer modeling approaches, and one that outlines our modeling approach.

Line 11: The Hibler (1979) reference belongs here.

➔ We have added a reference to Hibler (1979) here.

Page 2104 Line 15: "evaluate" not "validate"

➔ This is changed to "evaluate". Thank you.

Page 2105 Line 23: The concentration depends on location - this should be stated (or simply say "in our area of interest").

➔ We have now rephrased this as "the Arctic sea ice concentration is mostly below 80%".

Page 2108: Line 10: For 100% ice cover the free drift assumption you make previously breaks down so the analysis that follows is strictly speaking not valid. You should note this. I also strongly suggest comparing θ_{IOBL} at $\varphi = 1$ to e.g. θ_{IOBL} at $\varphi = 0.8$ and with different wind speeds in order to give the reader a sense of the variability in the solution at high ice concentration.

➔ As stated above, we have modified the text of this section to acknowledge that the 100% sea ice concentration is inconsistent with the free drift approximation, but provides a good approximation to the general model solution to for $\varphi \geq 0.5$..

Page 2109: Line 7: or, equivalently to the 10 m winds.

➔ Yes, this sentence is changed to "equivalently to the 10 m winds" – thank you.

Page 2110: Line 11: You provide an analytical solution but don't really use it - is this right? If so, then why is the analytical solution in the main text? Seems like it belongs in an appendix. - Turns out you do use equation (16) in the following text. In this case the text on page 2110 should reflect this better.

➔ This analytical solution is used for plotting the wind-ice and ice-ocean velocity angles (Figures 3 and 4). This analytical solution can provide physical insight into the IOBL turning angle, θ_{IOBL} (equation 20) and wind-ice velocity angle θ_{ai} (equation 21). We have emphasized the purpose of presenting the analytical solution at the start of section 2.

Line 17: Equation (17) looks like it could be an interesting result, but I find it hard to connect θ_{IOBL} and α and $|\mathbf{u}_0^*|^2$. A graph could be enlightening.

➔ As the reviewer suggests, we added a plot showing the sensitivity of θ_{IOBL} to α ($\alpha = \sqrt{2K_0^*/C_{io}}$) – this is presented as Fig.2 in the revised manuscript.

Page 2111 Line 16: It is not clear to me how $|\tau_{ai}| \to 0$ leads to $|\tau_{io}|/|\tau_{ai}| \to 0$

➔ We agree that this requires further explanation. To obtain this result from equation (16),

$$k_o^2|\vec{u}_{io}^*|^4 + 2k_o|\vec{u}_{io}^*|^3 + (1 + (\alpha + 1)^2)|\vec{u}_{io}^*|^2 = k_a^2|\vec{u}_{ai}^*|^4,$$

first note that if $|\vec{u}_{ai}^*| = 0$ then the only solutions for $|\vec{u}_{io}^*|$ are $|\vec{u}_{io}^*| = 0$ and

$$k_o^2|\vec{u}_{io}^*|^2 + 2k_o|\vec{u}_{io}^*| + (1 + (\alpha + 1)^2) = 0.$$

It is straightforward to show that this quadratic equation has no real and positive solutions, so the only possibility is that $|\vec{u}_{io}^*| \to 0$ as $|\vec{u}_{ai}^*| \to 0$. Now suppose that $|\vec{u}_{io}^*| = C|\vec{u}_{ai}^*|^p$ for some positive p as $|\vec{u}_{ai}^*| \to 0$. Substituting this ansatz into equation (16), we obtain

$$k_o^2C^4|\vec{u}_{io}^*|^{4p} + 2k_oC^3|\vec{u}_{ai}^*|^{3p} + (1 + (\alpha + 1)^2)C^2|\vec{u}_{ai}^*|^{2p} = k_a^2|\vec{u}_{ai}^*|^4 \quad \text{as} \quad |\vec{u}_{ai}^*| \to 0.$$

If p < 2 then as $|\vec{u}_{ai}^*| \to 0$ the third term on the left-hand side will become dominant, and the equality will be broken. If p > 2 then the term on the right-hand side will become dominant as $|\vec{u}_{ai}^*| \to 0$, and again the equality will broken. We conclude that $|\vec{u}_{io}^*| \sim |\vec{u}_{ai}^*|^2$ as $|\vec{u}_{ai}^*| \to 0$.
We have provided a brief explanation of this point in the text.

Line 21: You're not really *validating* the model, but rather *evaluating*. Validation implies that you're confirming that the model is right, which it cannot be in the strictest sense, since you employ a number of simplifications (and compare it with a reanalysis).
Evaluation implies that you're trying to find out how well the model performs, which is much more appropriate here. This comment holds whenever you use 'validating' for the rest of the text.

➔ Yes, as the reviewer suggests, we changed the word 'validate' to 'evaluate'.

Page 2112: Line 19: Why do you re-grid the SSMI data? Line 25: Do you use the mean thickness from the 12 categories? Line 27: Aren't winds always atmospheric?

➔ The ERA-Interim wind data is provided on a latitude/longitude grid, and so the ice velocities computed using our model are calculated on that grid. It is therefore more practical to interpolate the SSMI data onto the same grid for the purpose of computing sea ice advection using the modeled ice velocities.
With regard to the PIOMAS sea ice thickness, only the mean thickness is provided to users.
Yes, "atmospheric winds" is changed to "surface wind stress".

Page 2113: Line 20: Is it reasonable to assume φ = 1? Only if we know that there isn't much difference between the solution for φ = 1 and φ = 0.85.

➔ We have deleted this sentence.

Page 2114: Line 1: cover _the_ winter season

➔ This has been corrected as the reviewer suggests. Thank you.

Line 12: I would have used something slightly larger for ρ_o, e.g. 1026, which is the density of salt water at salinity of 32 and at the freezing point.

➔ We agree with the reviewer. In this revised manuscript, we used higher water density, $\rho_o = 1026\ \mathrm{kg/m^3}$ for all the calculations.

Line 14: Why do you have two values for C_{ai}?

➔ This is typo. The second C_{ai} should be changed to C_{ao}

"but for simplicity we use a constant values of $C_{ai} = 1.89 \times 10^{-3}$ and $C_{ao} = 1.25 \times 10^{-3}$".

Page 2115: Line 5: You should also mention the classical free drift case and how it compares to the observations (cf. section 6.1.1 in Matti Lepparanta's book).

➔ We have now added curves showing the 'classical free drift' case to figures 3a and 4a (solid blue line).

Line 17: This paragraph is too long and covers multiple topics. Please split it up.

➔ We have now split this paragraph up, moving the discussion of the figures comparing the modeled and observationally-derived wind-ice velocity angles to a separate following paragraph.

Page 2116: Line 18: "... suitable for _the_ marginal ice zone". Also, you have been focusing on $\varphi = 1$, not $\varphi \ll 1$. Line 19: I was very happy to see the plots in figure 4 and read your discussion of them. It feels like it comes a bit late though. Maybe adding a reference to this discussion in section 2.2 would suffice?

➔ As stated above, we have now explained earlier in the manuscript that the 100% sea ice concentration is inconsistent with the free drift approximation, but provides a good approximation to the general model solution to for $\varphi \geq 0.5$.

Page 2118: Line 5: Doesn't the PIOMAS thickness also show a trend that then needs to be removed?

➔ Yes, the PIOMAS sea-ice thickness shows a thinning trend, especially since 2005. However, the Arctic sea-ice thickness is poorly observed and PIOMAS thickness is known to have

substantial biases (Johnson et al. 2012; Schweiger et al. 2011). Therefore, it may not be reliable to use the time-varying sea-ice thickness from PIOMAS to calculate the wind-induced sea ice velocities. Instead, we used the climatological mean sea ice thickness.

Page 2119: Line 10: You got better results using K_0^* = 0.1 in the previous section - why didn't you use that value here?

➔ In this revised version of manuscript, we discuss that the improved fitting with a larger value of vertical diffusivity is because our model neglects the internal stress, which is likely to be large in ice concentrated regions (especially in winter).

Line 14: Which 10 day period?

➔ This sentence is rephrased as: "Over a 10 day period since the development of southerlies"

Page 2120: Line 5: Depending on the season you could also be seeing substantial ice melt - which is quite likely. The ice atmosphere drag could also be too low.

➔ In late summer it is likely that there is indeed substantial ice melt, acting to reduce the sea ice concentration in most areas of the Arctic. Our results show that there is a further, anomalous change in the sea ice concentration associated with ice drift due to southerly wind events in the Pacific sector.

Line 10: I suppose this is then the 'classical' free drift case? You should state this if that is the case.

➔ Yes. This sentence is rephrased as: "As introduced in Sec. 4, the 'classical' fee drift (zero Ekman layer velocity) corresponds mathematically to the limit of infinitely large vertical diffusivity ($K_o^* \to \infty$) in our model. In Fig. 9 we compare the anomalous sea-ice speed associated with the wind-induced free drift with and without an IOBL included in the model".

Line 21: You only show the results from one event, so you cannot claim that "the model demonstrate[s] that Arctic southerly wind events drive substantial reduction in sea ice concentration". If you throw a 'can' into this sentence, then we're fine.

➔ As explained above, we present results for a composite of 27 identified southerly wind strengthening events between 1990 and 2012. The agreement between our model's predictions and the observed sea ice concentration anomalies during these events supports this claim, so we have left this sentence essentially unchanged.

Page 2121: Line 10: It's true that using your model is much faster/efficient/easier than running a GCM, but you should have mentioned this earlier in a 'motivations paragraph' somewhere.

➔ As the reviewer suggests, we introduce this merit earlier in the introduction: "The analytical tractability of our model allows efficient calculation of the sea-ice drift, certainly much more so than running a full coupled model of the Arctic".

References

Sumata, H., T. Lavergne, F. Girard-Ardhuin, N. Kimura, M. A. Tschudi, F. Kauker, M. Karcher, and R. Gerdes.: An intercomparison of Arctic ice drift products to deduce uncertainty estimates, *J. Geophys. Res. Oceans*, **119**, 4887–4921, (2014).

Johnson, M., Proshutinsky, A. et al.: Evaluation of Arctic sea ice thickness simulated by Arctic Ocean Model Intercomparison Project models, *J. Geophys. Res*., **117**, C00D13, doi:10.1029/2011JC007257, 2012.

Schweiger, A., Lindsay, R., Zhang J., Steele M., Stern, H., and Kwok, R.: Uncertainty in modeled Arctic sea ice volume, *J. Geophys. Res*., **116**, C00D06, doi:10.1029/2011JC007084, 2011.

Response to Anonymous Reviewer #2

We thank the reviewer for their comments on our paper. We have revised the manuscript in accordance with these comments and those of the other reviewer. In particular, we added plots showing the effect of ice-ocean drag coefficient on ice speed (see Fig. 3). We added caveats in several places that our model may overestimate ice drift speed and velocity angles because the internal stress is neglected. Moreover we added a section (Sec 2.3) that discusses similarities and differences between our analytical model and Rossby similarity theory. We respond to the reviewer's comments individually below.

General comments:

The authors present an analytical model for the drift of sea ice that combines an ice-water "mixture layer" with an Ekman layer, which eliminates the need to specify the ice-ocean boundary layer turning angle. This model is applied to interpret ice-tethered profiler (ITP) observations, and summer Arctic ice edge retreat as a response to southerlies. Approaches like this one fill an important gap between modelling and observations in the ice-ocean boundary layer, where the former has always been the quadratic drag coefficient approach, and the latter has converged to a Rossby similarity approach with multiple stratification-dependent scalings, mainly due to the work of McPhee et al.

➔ We thank the reviewer for their encouraging words on our study.

The authors refer to Rossby similarity scaling several times. In my opinion, they could do a better job at pointing out the crucial differences between Rossby similarity and their approach: Rossby similarity combines a constant-stress (surface) layer (very little velocity turning) with the traditional Ekman spiral (45 degrees between velocity and stress for constant Ekman layer eddy viscosity). Because the height of the constant-stress layer scales with friction velocity (and thus ageostrophic ice drift), this leads to variations in both quadratic drag coefficient and turning angle (even for 100% ice cover).

➔ Following the reviewer's suggestion, we added a section (Sec. 2.3: Physical interpretation), discussing the similarities and difference between our equation and the equation derived from Rossby similarity theory for the case of close to 100% ice cover.

A crucial point that the model presented by the authors handles differently is that Rossby

similarity provides a framework (by means of the logarithmic constant-stress layer) to quantify the effect of changing surface roughness. The authors, on the other hand, simply use a constant ice-ocean drag coefficient, where the ice thickness comes in by way of changing the ice-momentum budget (air-sea momentum input going directly into the Ekman layer), as opposed to changing ice-ocean drag.

➔ This aspect of our model is indeed different from previous work on the ocean-ice boundary layer and Rossby similarity theory. Though conceivably Rossby similarity theory could be extended to describe the ice-ocean boundary layer in the presence of open water between the sea ice flows, to our knowledge no such extension has been performed. Yet in summer, sea ice conditions the presence of open water makes a leading contribution to the momentum transfer from the atmosphere to the ocean. We therefore assumed quadratic drag laws at the atmosphere-ice, atmosphere-ocean, and ice-ocean interfaces for simplicity, with the understanding that much work remains to be done to derive a more rigorous treatment of the ocean surface boundary layer in the spirit of Rossby similarity theory. We have provided additional discussion of this point in the new section 2.3.

The authors provide figures that show the variation in ice-ocean turning angle with drift speed, but none that shows the variation of the quadratic drag coefficient with drift speed (or alternatively, drift speed vs. interface stress). I feel that the drag coefficient is a better way to constrain model validity, both since turning angles are notoriously noisy (confounded by inertial motions and unsteady forcing) and since drag coefficients (i.e. drift speeds) have more to say about the relative drift patterns than relatively small variations in turning angles. In addition, such a plot would provide another measure to gauge the validity of the study's approach against e.g. Rossby similarity and data from e.g. AIDJEX.

➔ We added a plot showing the sensitivity of ice drift speed to varying ice-ocean drag coefficient (now Fig. 3). The analytical model with the canonical value of vertical eddy diffusivity $K_o^* = 0.028$ and the ice-ocean drag coefficient $C_{io} = 0.0071$ somewhat overestimates the observed ice drift speed. We added a discussion that this is probably because our model neglects the internal stress that impedes sea-ice drift in the relatively concentrated sea ice (higher than 85-95% in Beaufort Sea in winter).

We agree with reviewer that the ice-ocean drag coefficient C_{io} would be useful measures for comparison with previous work. It is difficult to calculate C_{io} accurately from the ITP-V data because the shallowest data is 6 m, which is a few meters below the ice base. However, in the appendix we calculated C_{io} following Cole et al. (2014) and plotted C_{io} as a function of surface

stress (Fig. A1). We could not identify any obvious dependence of C_{io} to surface stress, so we simply use the constant value $C_{io} = 0.0071$ suggested by Cole et al. (2014).

As the authors state, stratification will have a lot to say about the turbulent transfer of momentum in the boundary layer. No plots or numbers are presented that could give an idea about the stratification regime - plots of sigma-theta covering the mixed layer and upper pycnocline would help the reader to assess stability, mixed-layer depth etc. Alternatively, the authors could summarize the right numbers and plots from Cole et al., 2014, if only for mixed-layer depths and the like.

➔ Rather than reproduce the work of Cole et al. (2014), we have followed the reviewer's suggestion and summarized the relevant plots from their paper in our section 4.

It is hardly surprising that southerly winds drive a decrease of sea ice concentration in the MIZ (and I am not entirely convinced yet that the author's model predicts this significantly better than other suitably tuned ice drift models).

➔ We think it is intuitive that short bursts of southerly wind stress driving against a sea ice concentration that increases northward leads to a reduction in sea ice concentration across much of the Arctic. However, to the best of our knowledge, this effect has not been reported previously. Instead, previous studies suggest that the development of Arctic anticyclone is a major cause of sea ice reduction in the summer (see Ogi and Wallace, 2007).

One problem that is not addressed is that on-ice winds tend to compact the ice, which might create internal ice stresses and thus interfere with the model's assumptions. The authors should discuss this source of error.

➔ Following the reviewer's suggestion, we added a note: "The increase in SIC over the Atlantic sector associated with cross-polar flow is also slightly underestimated. Over the Atlantic sector, the cross-polar flow increases SIC and the internal stress is likely to increase as well. As mentioned earlier, our analytical model neglects internal stress that can decelerate ice drift and pile up sea ice over the Atlantic sector".

In general, it would be favorable to have some sort of handle on the error the authors make by assuming no internal ice stresses. See more concrete comments below. I do understand that this can be challenging. It is difficult to see without further quantification, however, how a free-drift approximation in the Beaufort in winter is good enough to e.g. allow for tuning the

nondimensional eddy Ekman viscosity K_0.

➔ It is indeed difficult to quantify the error associated with the neglect of the internal stress, and we are unable to do so within the scope of this paper. However, Cole et al. (2014) note that the wind-to-ice speed ratio is much larger than was found in AIDJEX, and is almost consistent with free drift. We have now included a discussion at the start of section 4 to the effect that the winter Beaufort Sea is not ideal for the purpose of evaluating the model because internal stresses may be dynamically significant, but that these observations appear to be closer to the free drift regime than might be expected of winter ice in this area.

I feel the article could be substantially improved by a more thorough discussion of the differences of the model from e.g. "traditional" Rossby scaling, which includes both limitations and possible improvements, in addition to the comments I have raised above. However, this article tackles an important issue and the material deserves to be exposed both to the modelling and the experimental community working on momentum transfer in the ice-ocean boundary layer, given that a suitable revision is made.

➔ As mentioned above, we have now included an additional section 2.3 to discuss these differences and the relative merits of both approaches.

Concrete comments:

p. 2103

l. 6 "over the ice-covered Arctic Ocean"

➔ Following the reviewer's comment, this sentence is rephrased as: "The synoptic eddy surface winds result in a primary mode of upper-ocean velocity variability with a period of 2-5 days over the ice-covered the Arctic Ocean (Plueddemann et al., 1998)".

l. 27 I would not call it straightforward since with Rossby similarity, you would lose the explicit description of the ice-ocean interface drag coefficient. But I agree that it is certainly possible.

➔ 'straightforward' has been changed to 'possible'.

p. 2107

l. 12ff. Rossby similarity, at least in the form given by McPhee, e.g. 2008, is hardly applicable to open-water problems. This has only to do with changing the boundary conditions between free surfaces and rigid floes because Rossby similarity's constant stress layer is based on scalings in the flow over rigid surfaces, so your statement confounds two issues here.

➔ We had intended to communicate exactly this sentiment, but evidently this paragraph was unclear. We have now stated clearly that Rossby similarity theory is not applicable to a mixture of sea ice and open water without substantial modification.

p. 2110

l. 23ff. Again, the drag coefficient varies, too (and more with surface roughness, not only with drift speed), and this is more crucial than the change in turning angle.

➔ As mentioned earlier, we have now calculated C_{io} following Cole et al. (2014) and plotted C_{io} as a function of surface stress (Fig. A1) – in the appendix. We have taken the simplest approach by assuming a constant C_{io} in all of our calculations because would prefer to avoid excessive tuning of the model parameters. We nevertheless find a close agreement between the model predictions and the observations.

p. 2113

l. 4, and in a few other instances: You probably mean model "evaluation" rather than "validation".

➔ Yes, "validation" is changes to "evaluation". Thank you for pointing this out.

l. 23 check grammar in this sentence ("observational fits to").

➔ This sentence is changed to "Extensive measurements of the ice-ocean boundary layer" – thank you for pointing this out.

p. 2114

l. 5 is this K=0.1 value just an educated guess or is there some least-squares regression behind this? You might mention that for rapid freezing, an altogether different outer layer scaling is appropriate ($\lambda \sim c_{ml} z_p$, where c_{ml} a constant and z_p pycnocline depth, see McPhee 2008), so tuning the eddy diffusivity would be more of an integrating scaling for the mixture of the outer boundary layer of the open water/floes mixture if this is what the authors intended to do.

➔ This is not a least-squares fit to the data, but rather a nominal value selected because it better explains the observational data. We do not attempt to claim that the larger K_o^* is necessarily more appropriate than the canonical $K_o^* = 0.028$, and we have now attempted to make this clearer in the text. Rather, we agree with the reviewer that the discrepancy between the observations and the model predictions is likely due to the influence of internal stress.

l. 16 this value of C_{io} was derived for 6 m depth, which is a couple of meters under the ice,

regardless of surface layer scaling height, and therefore strictly speaking not applicable as drag coefficient between ice and top of the Ekman layer. This could be mentioned. (The numerical value is probably good for this application, though.)

➔ Yes, we agree with reviewer. We have now added a sentence to explain this caveat.

l. 26f. I would guess that non-free drift is a much more likely reason than a possible wrong tuning of K_0 . Neither Stern & Lindsay, JGR 2009 (large b values) or Kwok et al., JGR 2013 (relatively small _ values) seem to indicate that free drift is a good approximation for this region in winter. Do your data allow you to make any inference about whether you had free drift?

➔ As mentioned in comments above, Cole et al. (2014) indicate that the ice is remarkably close to a free drift regime for the winter Beaufort Sea. However, we agree with the reviewer that the discrepancy is still more likely due to the influence of internal stress, and we have modified the text to reflect this.

p. 2116

l. 25 please indicate how this can be inferred from Eq. 18.

➔ In this revised manuscript, Eq 18 is changed to Eq 21. This sentence is rephrased as: "It can therefore be inferred from equation (21) and Fig. 6a that thicker ice has smaller stress ratio $|\vec{\tau}_{io}|/|\vec{\tau}_{ai}|$, implying that thicker ice is less efficient in transferring the momentum into the ocean, leading to larger wind-ice velocity angle".

p. 2118

l. 22 use either d (differential eqn.) or _ (difference eqn.) - don't mix them.

➔ Following the reviewer's suggestion, the notation of this equation has been changed. Please see Equation (24).

p. 2119

l. 10 do you also use the same C_{io} as for the ITP-V observations? This might be a source of error.

➔ Yes, this sentence is rephrased as: "All of the analytical model results presented here use the canonical value of vertical diffusivity ($K_o^* = 0.028$) and the ice-ocean drag coefficient of $C_{io} = 0.0071$ (Cole et al., 2014). As shown in Fig. 3, the wind-induced ice speed is sensitive to both K_o^* and C_{io}".

p. 2120

l. 1 Do you have any indications that PIOMAS overestimates sea-ice thickness?

➔ We added a reference indicating that PIOMAS overestimates sea-ice thickness: "While PIOMAS simulates the Arctic sea-ice thickness within a reasonable range, the model is known to generally *overestimate the thickness* of measured sea ice thinner than 2 m (Johnson et al. 2012; Schweiger et al. 2011)".

l. 3 It almost certainly is, see scaling for positive buoyancy fluxes in McPhee, 2008.
What you neglect, however, is that C_{io} might be different, too - both reduced turbulent drag due to freshwater layers in the surface (e.g. Randelhoff et al. 2014, JPO or McPhee et al. 1989, JGR) and a different ice roughness/form drag/internal wave drag regime.

➔ Thank you for the additional references. We have now acknowledged that changes in the surface layer composition and drag regime could also modify the drag coefficient in summer, providing another potential source of error.

l. 10 Did you increase C_{io} for this one accordingly? As I understand it, just setting the ocean surface velocity (at the top of the Ekman layer) to zero would correspond to setting the Ekman layer drag (or, equivalently, K_0) to infinity, and it's hardly surprising that lower drag enhances the ageostrophic ice speed.

➔ We prescribed a constant ice-ocean drag coefficient, $C_{io} = 0.0071$. We understand that this result is intuitive. However, we believe this study quantifies for the first time that the ice-ocean boundary layer (IOBL) enhances the wind-induced sea-ice speed by 50%.

References

Cole, S. T., Timmermans, M-L., Toole, J. M., Krishfield, R. A., and Thwaites, F. T.: Ekman Veering, Internal Waves, and Turbulence Observed under Arctic Sea Ice, *J. Phys. Oceanogr*., **44**, 1306–1328, 2014.

Ogi, M. and Wallace, J. M.: The role of summer surface wind anomalies in the summer Arctic sea ice extent in 2010 and 2011, *Geophys. Res. Lett*., **39**, L09704, 2012.

Johnson, M., Proshutinsky, A. et al.: Evaluation of Arctic sea ice thickness simulated by Arctic Ocean Model Intercomparison Project models, *J. Geophys. Res*., **117**, C00D13, doi:10.1029/2011JC007257, 2012.

Schweiger, A., Lindsay, R., Zhang J., Steele M., Stern, H., and Kwok, R.: Uncertainty in modeled Arctic sea ice volume, *J. Geophys. Res*., **116**, C00D06, doi:10.1029/2011JC007084, 2011.

An analytical model for wind-driven Arctic summer sea ice drift

H.-S. Park[1] and A. L. Stewart[2]

[1]{Korea Institute of Geoscience and Mineral Resources, Daejeon, South Korea}

[2]{Department of Atmospheric and Oceanic Sciences, University of California, Los Angeles}

Correspondence to: H.-S. Park (hspark1@gmail.com)

Abstract

The authors present an ~~approximate~~ analytical model for wind-~~induced sea-ice~~ driven free drift of sea ice that allows for an arbitrary mixture of ice and open water. The model includes an ice-ocean boundary layer with an Ekman spiral ~~in~~, forced by transfers of wind-input momentum both through the ~~ocean velocity. This model provides an analytically tractable solution that is most applicable to the marginal ice zone, where~~ sea-ice ~~concentration is substantially below 100%. The model closely reproduces~~and directly into the open water between the ice ~~and upper-ocean velocities observed recently by the first ice-tethered profiler equipped with a velocity sensor (ITPV).~~ floes. The analytical tractability of ~~our~~this model allows efficient calculation of the ~~sea~~ ice velocity provided that the surface wind field is known and that the ocean ~~surface~~ geostrophic velocity is relatively weak. The model ~~is applied to estimate intraseasonal~~ predicts that variations in ~~Arctic sea ice cover due to short timescale (around 1 week) intensification of~~ the ice thickness or concentration should substantially modify the ~~southerly winds. Utilizing 10 m surface winds from ERA-Interim reanalysis,~~ rotation of the ~~wind-induced sea-ice~~ velocity ~~and~~between the ~~associated changes in sea-ice concentration are calculated and compared with satellite observations. The analytical model captures the observed reduction of Arctic sea-ice concentration associated with~~ 10m winds, the sea ice, and the ~~strengthening of southerlies on intraseasonal time scales. Further analysis indicates that~~

~~the wind-induced surface Ekman flow in the ocean increases the sea-ice drift speed by 50% in the Arctic summer. It is proposed that the southerly wind-induced sea-ice drift, enhanced by the ocean's surface Ekman transport, can lead to substantial reduction in sea-ice concentration over a timescale of one week.~~ocean.

The model is evaluated against recent observational data from the first ice-tethered profiler equipped with a velocity sensor (ITP-V). Though these observations were made in winter when internal stresses in the ice are likely to have been dynamically significant, our model is largely able to capture the dependence of the ice speed and the wind/ice/ocean turning angles on the wind speed. The model is then used to show that strengthening of the southerlies on intraseasonal time scales (around 1 week) reduces summer sea ice concentration in the Pacific sector via wind-induced sea ice drift. The 10m winds from ERA-Interim reanalysis are used to model the sea ice drift induced by 27 southerly intensification events between 1990 and 2012. The resulting anomalous changes in sea ice concentration are calculated and found to compare closely with satellite observations.

1 Introduction

~~The drift of Arctic sea ice~~ is largely explained by surface winds and upper~~-~~-ocean currents. The effect of the mean geostrophic upper-ocean ~~current~~currents on the average circulation of sea~~-~~ ice pack is known to be as important as the mean wind field (~~Hibler 1979;~~ Thorndike and Colony, 1982). However, the role of the winds becomes increasingly important over shorter time scales: On time scales from days to months, surface wind variability ~~explain~~explains more than 70% of the sea~~-~~ ice motion (Thorndike and Colony, 1982), and is well correlated with the surface ocean velocity (Cole et al., 2014~~; Kawaguchi and Mitsudera, 2008).~~). The synoptic eddy surface winds result in a primary mode of upper-ocean velocity variability with a period of 2~~-~~5 days ~~in~~over the ~~Pacific and Canadian sectors of the~~ice-covered Arctic Ocean (Plueddemann et al., 1998). The tight connection between surface winds and upper ocean velocity over ice-covered Arctic Ocean suggests that resolving the ~~eddy~~ wind-induced surface Ekman flow is essential for simulating sea~~-~~ ice motions.

Many simple sea- ice models assume steady ocean currents and prescribe a quadratic relationship with an empirically-chosen turning angle between the ice stress and surface ocean ~~current (~~velocity (Hibler 1979; Thorndike and Colony, 1982; Bitz et al., 2002; Liu et al., 2011; Uotila et al., 2012). This ~~simple~~ model configuration has limitations in simulating wind-induced sea- ice drift on intraseasonal time scales, during which time-varying Ekman layer flows in the ice-ocean boundary layer (IOBL) may be important. The effect of the surface Ekman flow on sea- ice motion can be resolved by coupling the sea- ice model to a comprehensive ocean model (Zhang and Rothrock, 2003; Uotila et al., 2012). However, such an approach is computationally expensive, and makes it difficult to disentangle the physical processes controlling sea- ice drift.

In the past few decades, considerable advances have been made in understanding the physics of the IOBL, notably via the development of Rossby similarity theory (McPhee, 1979; 1981; 1994; 2008). In the case of an unstratified surface layer, this theory connects the ocean's Ekman layer to the ice base via a thin surface layer in which the velocity shear follows the *law of the wall* and the vertical eddy viscosity varies linearly to zero. In contrast to frequently-used quadratic drag parameterizations (e.g. Hibler 1979; Thorndike and Colony, 1982), this results in a quadratic drag coefficient and turning angle that depend on the stress velocity and the hydraulic roughness length of the ice base. However, the assumptions underlying Rossby similarity theory make it inapplicable to the case of a mixture of sea ice and open water, which is typical of the Arctic in summer.

In Sec. ~~study,~~2 we derive an approximate analytical ~~solution~~ model for wind-induced sea- ice drift that accounts for the Ekman spiral in the IOBL~~.~~ and allows for an arbitrary mixture of ice and water, but neglects internal stress within the ice. The model is therefore most appropriate to the marginal ice zone which covers much of the Arctic during summer. This ~~analytical model~~ approach has ~~merits~~ both ~~in~~ theoretical and practical ~~aspects. Because~~merits: because the Ekman layer is resolved in the momentum balance, the turning angle is a prognostic variable in our model~~. Our model therefore provides an interpretation of recent observations on Arctic sea ice motions from an ice-tethered profiler (Cole et al., 2014), in particular the angles between the wind and ice velocities and between the ice and ocean velocities. Our treatment of the IOBL is~~

~~conceptually similar to Rossby similarity theory (McPhee, 1979; 1981; 1994; 2008). We employ a somewhat simpler treatment of the momentum transfer from the sea ice to the IOBL, but it is straightforward to extent our solution to incorporate Rossby similarity theory. The analytical tractability of our model allows efficient calculation of the sea-ice drift, given the surface wind velocity. Moreover, this model allows for an arbitrary mixture of sea ice and water, and is therefore suitable for application to the marginal ice zone~~, allowing us to explore the dependence of both the ice drift speed and the wind/ice/ocean turning angles on the concentration and thickness of the sea ice. The analytical tractability of the model allows efficient calculation of the sea ice drift, certainly much more so than running a full coupled model of the Arctic. We exploit this efficiency to compare our model's predictions against observations of Arctic sea ice concentration and velocity: the data sources and reanalysis products used for this purpose are described in Sec. 3.

In Sec. ~~We use this analytical model to quantify wind-driven intraseasonal variability of sea-ice cover.~~4, we evaluate our model against recent observations from an ice-tethered profiler (Cole et al., 2014), focusing on the angles between the wind and ice velocities and between the ice and ocean velocities. At face value our model may not appear to be applicable to this data because the measurements were made in the Beaufort Sea in winter, when the sea ice concentration is close to 100% and internal stress is likely to be dynamically significant (Leppäranta, 2005). However, the analysis of Cole et al. (2014) suggests that the ice floe velocity was in fact close to a free drift regime, and that the vertical buoyancy flux in the IOBL was small, compared to previous winter observations (see *e.g.* McPhee, 2008). Consequently our model is largely captures the dependence of the ice speed and turning angle on the surface wind speed.

In Sec. 5 we apply our model to predict the anomalous change in Arctic sea ice concentration associated with intraseasonal intensification of the southerly winds in the Pacific sector. This serves a dual purpose: First, it is a test of our model's assumptions that the summer sea ice drift can be described accurately by neglecting internal stresses and assuming constant drag coefficients at the ice-ocean, atmosphere-ice, and atmosphere-ocean interfaces. Second, by extension, it tests the hypothesis that the

anomalous reduction in sea ice concentration in the Pacific sector during southerly wind events can be attributed to the mechanical effect of wind-driven ice drift, rather than thermodynamic effects. Many previous observational analyses provided only statistical connections between the southerly winds and sea- ice cover. For example, the strength of south-westerlies over the Barents Sea is well correlated with sea- ice cover in winter (Sorteberg and Kvingedal, 2006; Liptak and Strong, ~~2013~~2014) and the development of anomalous southerlies over the Pacific sector of the Arctic is often followed by a reduction of sea- ice cover in the spring and summer (Wu et al., 2006; Serreze et al., 2003). ~~In this study, we hypothesize~~We demonstrate that the southerly wind-induced sea-ice advection, accelerated by wind-induced surface Ekman flow, can substantially decrease sea- ice concentration over ~~the course~~a time scale of ~~a~~ one week ~~or so. The structure of this paper is as follows. In Sec. 2, we derive an approximate analytical solution for the sea-ice velocity, including an Ekman spiral in the IOBL. .In Sec. 3, we describe the data sources and reanalysis products used in this study. In Sec. 4, we validate our model by comparing the analytically-derived wind–ice and ice–ocean velocity angles against recent observations from an ice-tethered profiler. Finally, in Sec. 5 we apply our model to quantify the impact of strong southerly wind events in the Arctic summer on the intraseasonal variability of sea-ice cover.~~

2 An analytical model for wind-driven sea- ice motion

In this section we employ a simplified sea- ice model to obtain analytical expressions for the sea- ice velocity as a function of surface wind speed. In Sec. 2.1 we formulate an approximate sea- ice momentum balance appropriate for basin-scale motions, and then in Sec. 2.2 we derive an analytical solution for the sea- ice velocity, assuming that the surface wind speed is known.

2.1 Model formulation

We employ a “mixture layer” model of Arctic sea ice (Gray and Morland, 1994), which describes the evolution of ice floes interspersed with patches of open water. The thickness-integrated momentum balance for such a mixture layer may be written as (Heorton et al., 2014),

$$\rho_i h_i \frac{D\vec{u}_i}{Dt} = \varphi(\vec{\tau}_{ai} - \vec{\tau}_{io}) - \rho_i h_i f\left(\hat{Z} \times \vec{u}_i\right) - \rho_i h_i g \nabla\eta + \nabla \cdot \boldsymbol{\sigma}. \quad (1)$$

where h_i is the ice thickness, ρ_i is the ice density, $\vec{u}_i$ is the ice velocity vector, η is the sea surface height, φ is the sea ice fraction, f is the Coriolis parameter, g is the acceleration due to gravity, and $\hat{Z}$ is a vertical unit vector. Equation (1) states that the ice/water mixture layer is accelerated by momentum exchanges between the ice and the atmosphere ($\vec{\tau}_{ai}$) and between the ice and the ocean ($\vec{\tau}_{io}$), by the Coriolis force, by horizontal pressure variations due to sea surface tilt, and by the divergence of a stress tensor ($\boldsymbol{\sigma}$) representing internal ~~friction~~stress in the ice.

We first write the lateral pressure gradient term in terms of the ocean near-surface geostrophic velocity $\vec{u}_g$,

$$f\hat{Z} \times \vec{u}_g = \rho_i h_i g \nabla\eta. \quad (2)$$

We are concerned with sea ice evolution over a typical time scale 1 week with a velocity scale of around 0.2 m/s, implying a length scale of around 100 km. The ice acceleration term in (1) may therefore be safely neglected (McPhee 1980; Thorndike and Colony, 1982). This precludes the sea ice undergoing inertial oscillations, though the diameter of such oscillations would only be a few km at most, much smaller than the drift length scale of 100 km. In summer, the Arctic sea- ice concentration is ~~typically~~mostly below 80~~%,~~% (see Fig. 1), so away from coastal shear margins the internal friction term in (1) is also negligible (Leppäranta, 2005; Kawaguchi and Mitsudera, 2008). This simplifies the momentum balance to

$$\rho_i h_i f\hat{Z} \times \left(\vec{u}_i - \vec{u}_g\right) = \varphi(\vec{\tau}_{ai} - \vec{\tau}_{io}), \quad (3)$$

Similar scaling arguments suggest that the pressure gradient due to the sea surface tilt may also be negligible. For now we retain this term because it is analytically tractable, but in Secs. 4 and 5 below, we will neglect the geostrophic ocean velocity term in (3).

Equation (3) states that the shear between the mixture layer and the ocean's surface geostrophic velocity, or equivalently the total shear across the ice-ocean boundary layer

(IOBL; McPhee, 2012) lies perpendicular to the vertical stress divergence in the sea ice. This equation does not account for momentum imparted from the winds to the water between the ice floes in the mixture layer, which is assumed to be transferred directly to the ocean below (Gray and Morland, 1994). The total stress felt by the ocean at the base of the mixture layer is therefore

$$\vec{\tau}_o = (1-\varphi)\vec{\tau}_{ao} + \varphi\vec{\tau}_{io}, \qquad (4)$$

where $\vec{\tau}_{ao}$ is the momentum imparted to the ocean from the atmosphere between the sea ice floes. We adopt an approach similar to Rossby similarity theory for the IOBL, assuming that the ocean velocity follows an Ekman spiral beneath the mixture layer (McPhee, 2012). The ocean velocity at the top of the Ekman layer is therefore given as

$$\vec{u}_o - \vec{u}_g = \frac{1}{\sqrt{2K_o^*}}\left(\vec{u}_o^* - \hat{Z}\times\vec{u}_o^*\right), \qquad (5)$$

where $K_o^* = Kf/|\vec{u}_o^*|^2$ is the dimensionless vertical eddy diffusivity, K is the dimensional vertical eddy diffusivity, $\vec{u}_o^*$ is a stress velocity defined by $\vec{\tau}_o = \rho_o|\vec{u}_o^*|\vec{u}_o^*$, and ρ_o is the ocean surface density. The dimensionless diffusivity K_o^* is taken to be constant, reflecting a linear dependence of the Ekman layer depth on the stress velocity. This is appropriate for IOBLs with no surface buoyancy forcing; non-zero surface buoyancy modifies the vertical profile of K in the IOBL (McPhee, 2008). Our model could be extended to accommodate an arbitrary K-profile if the surface buoyancy fluxes were known, but for simplicity in this study we assume zero surface buoyancy forcing.

We prescribe the air–ice, air–ocean, and ice–ocean stresses using quadratic drag relations,

$$\vec{\tau}_{ai} = \rho_a C_{ai}|\vec{u}_a|\vec{u}_a = \rho_a|\vec{u}_{ai}^*|\vec{u}_{ai}^*, \qquad (6a)$$

$$\vec{\tau}_{ao} = \rho_a C_{ao}|\vec{u}_a|\vec{u}_a = \rho_a|\vec{u}_{ao}^*|\vec{u}_{ao}^*, \qquad (6b)$$

$$\vec{\tau}_{io} = \rho_o C_{io}|\vec{u}_i - \vec{u}_o|(\vec{u}_i - \vec{u}_o) = \rho_o|\vec{u}_{io}^*|\vec{u}_{io}^*. \qquad (6c)$$

where ρ_a and ρ_o are the atmospheric and surface ocean density respectively. Here we have implicitly assumed that there exist thin turbulent boundary layers between the

atmosphere and the ice floes, between the atmosphere and ocean leads, and between the bases of the ice floes and the top of the Ekman layer, all of which transfer momentum at a rate that varies quadratically with the vertical shear. We have further assumed that any momentum imparted to the ocean leads is transferred directly down to the Ekman layer below. More comprehensive treatments of the ice–ocean stress may be derived using Rossby similarity theory (McPhee 2008; 2012). However, ~~application of~~ this theory ~~becomes complicated by~~cannot be applied in the presence of leads between the sea ice floes, which continually change the surface boundary condition at any given point between a free surface and a rigid ice floe. In many previous studies, these stresses carry a turning angle to account for the effect of the Coriolis force in the boundary layer (Hibler 1979; Thorndike and Colony 1982; Bitz et al. 2002; Uotila et al. 2012). This is not necessary here because we use the ageostrophic 10-m winds, and we explicitly account for the ocean surface Ekman layer.

By combining the ice–ocean stress relation (6c), which can be rewritten as $\vec{u}_{io}^{*} = \sqrt{C_{io}}(\vec{u}_i - \vec{u}_o)$, with equation (5) for the shear across the Ekman layer, we obtain an expression for the total shear across the IOBL,

$$\vec{u}_i - \vec{u}_g = \frac{1}{\sqrt{C_{io}}}\vec{u}_{io}^{*} + \frac{1}{\sqrt{2K_0^{*}}}\left(\vec{u}_o^{*} - \hat{Z} \times \vec{u}_o^{*}\right). \tag{7}$$

Then, substituting (6a), (6c) and (7) into the momentum balance (3), we obtain a relationship between the unknown stress velocities $\vec{u}_{io}^{*}$ and $\vec{u}_o^{*}$,

$$\frac{\rho_i h_i f}{\sqrt{C_{io}}}\hat{Z} \times \vec{u}_{io}^{*} + \frac{\rho_i h_i f}{\sqrt{2K_0^{*}}}\left(\hat{Z} \times \vec{u}_o^{*} + \vec{u}_o^{*}\right) = \varphi(\rho_a |\vec{u}_{ai}^{*}| \vec{u}_{ai}^{*} - \rho_o |\vec{u}_{io}^{*}| \vec{u}_{io}^{*}). \tag{8}$$

We require an additional equation to obtain an explicit solution for $\vec{u}_{io}^{*}$ and $\vec{u}_o^{*}$, so we rewrite the total stress at the base of the mixing layer (4) in the form

$$\rho_o |\vec{u}_o^{*}| \vec{u}_o^{*} = (1 - \varphi)\rho_a |\vec{u}_{ao}^{*}| \vec{u}_{ao}^{*} + \varphi \rho_o |\vec{u}_{io}^{*}| \vec{u}_{io}^{*}. \tag{9}$$

2.2 Model solution

We now solve equations (8) and (9), derived in the previous subsection, ~~analytically~~ for the stress velocities $\vec{u}_{io}^*$ and $\vec{u}_o^*$, and thus for the ice velocity $\vec{u}_i$. ~~In this subsection we focus on the simplest case of~~

2.2.1 Near-100% sea ice cover (~~$\varphi = 1$~~). In~~$\boldsymbol{\varphi \approx 1}$~~)

We first consider the case of close to 100% sea ice cover ($\varphi \approx 1$) because this permits a closed-form analytical solution that offers physical intuition for the behavior of the model. Though an actual sea ice concentration of 100% would be inconsistent with our model, we will show in Sec. 4 that this ~~case the~~provides a close approximation to the general solution for ice concentrations greater than 50%. The method of solution is very similar to that described by Leppäranta (2005), Ch. 6.1, but our explicit treatment of the oceanic boundary layer and prognostic determination of the turning angle warrant that the solution be given in full. ~~In the Appendix we discuss the solution for the general case of partial~~

~~For~~ sea ice ~~cover~~concentrations close to 100% (φ ~~$=$~~≈ 1~~), which is substantially more complicated. For $\varphi = 1$,~~ equation (9) ~~simplifies to~~ implies that the ice-ocean and ocean surface stress velocities are approximately equal, $\vec{u}_{io}^*$ ~~$= \vec{u}_o^*$~~, ~~and thus~~ $\approx \vec{u}_o^*$. Thus equations (7) and (8) may be rewritten as

$$\vec{u}_i - \vec{u}_g = \left(\frac{1}{\sqrt{C_{io}}} + \frac{1}{\sqrt{2K_0^*}}\right)\vec{u}_{io}^* - \frac{1}{\sqrt{2K_0^*}}\hat{Z} \times \vec{u}_{io}^*, \tag{10a}$$

$$\left(\frac{\rho_i h_i f}{\sqrt{2K_0^*}} + \frac{\rho_i h_i f}{\sqrt{C_{io}}}\right)\hat{Z} \times \vec{u}_{io}^* + \frac{\rho_i h_i f}{\sqrt{2K_0^*}}\vec{u}_{io}^* = \rho_a |\vec{u}_{ai}^*|\vec{u}_{ai}^* - \rho_o |\vec{u}_{io}^*|\vec{u}_{io}^*. \tag{10b}$$

We simplify the coefficients by multiplying both sides of (10b) by $\sqrt{2K_0^*}/\rho_i h_i f$ and rearranging to obtain

$$(\alpha + 1)\hat{Z} \times \vec{u}_{io}^* + (1 + k_o|\vec{u}_{io}^*|)\vec{u}_{io}^* = k_a|\vec{u}_{ai}^*|\vec{u}_{ai}^*, \tag{11}$$

where $\alpha = \sqrt{2K_0^*/C_{io}}$, $k_a = \rho_a\sqrt{2K_0^*}/\rho_i h_i f$ and $k_o = \rho_o\sqrt{2K_0^*}/\rho_i h_i f$ (12)

To solve, we first define the components of $\vec{u}_{io}^*$ parallel and perpendicular to the wind

stress velocity, or, equivalently, perpendicular the 10 m winds:

$$u_{io}^{*\parallel} = \frac{\vec{u}_{ai}^{*}}{|\vec{u}_{ai}^{*}|} \cdot \vec{u}_{io}^{*}, \tag{13a}$$

$$u_{io}^{*\perp} = \left(\hat{Z} \times \frac{\vec{u}_{ai}^{*}}{|\vec{u}_{ai}^{*}|}\right) \cdot \vec{u}_{io}^{*}. \tag{13b}$$

Then taking the dot product of $\vec{u}_{io}^{*}$ with both sides of equation (11) and rearranging yields an expression for $u_{io}^{*\parallel}$,

$$u_{io}^{*\parallel} = \frac{1}{k_a} \frac{|\vec{u}_{io}^{*}|^2}{|\vec{u}_{ai}^{*}|^2} (1 + k_o |\vec{u}_{io}^{*}|), \tag{14}$$

while taking the dot product of $\hat{z} \times \vec{u}_{io}^{*}$ with both sides of (11) yields an expression for $u_{io}^{*\perp}$,

$$u_{io}^{*\perp} = -\frac{1}{k_a} \frac{|\vec{u}_{io}^{*}|^2}{|\vec{u}_{ai}^{*}|^2} (1 + \alpha). \tag{15}$$

Equations (14) and (15) do not constitute an explicit solution for $\vec{u}_{io}^{*}$ because they depend on the magnitude $|\vec{u}_{io}^{*}|$. We determine this magnitude using the definition, $|\vec{u}_{io}^{*}|^2 = \left(u_{io}^{*\parallel}\right)^2 + (u_{io}^{*\perp})^2$, which yields a quartic equation for $|\vec{u}_{io}^{*}|$,

$$k_o^2 |\vec{u}_{io}^{*}|^4 + 2k_o |\vec{u}_{io}^{*}|^3 + (1 + (\alpha + 1)^2) |\vec{u}_{io}^{*}|^2 = k_a^2 |\vec{u}_{ai}^{*}|^4. \tag{16}$$

In principle, this may be solved analytically for $|\vec{u}_{io}^{*}|$, but for the purposes of this study we solve (11) numerically. Note that the right-hand side of (11) is a monotonically increasing function of $|\vec{u}_{io}^{*}|$, so a unique solution exists for any wind stress velocity $|\vec{u}_{ai}^{*}|$. Having obtained the components of the stress velocity, it is straightforward to solve for the shear between the sea ice and the geostrophic ocean velocity using (10a).

2.2.2 Sparse sea ice cover ($\varphi \ll 1$)

We now consider sea ice concentrations much below 100%, for which it is would be inaccurate to assume $\varphi \approx 1$. In general there is no closed-form analytical solution to the model equations, and a solution must be obtained numerically. We begin by simplifying the coefficients in equations (8) and (9) by defining α, k_a, and k_o as in Sec. 2.1, and

additionally defining $\beta = \rho_a C_{ao}/\rho_o C_{ai}$.

$$\alpha\hat{Z} \times \vec{u}_{io}^{*} + \hat{Z} \times \vec{u}_{o}^{*} + \vec{u}_{o}^{*} = \varphi k_a |\vec{u}_{ai}^{*}|\vec{u}_{ai}^{*} - \varphi k_o |\vec{u}_{io}^{*}|\vec{u}_{io}^{*}, \quad (17)$$

$$|\vec{u}_{o}^{*}|\vec{u}_{o}^{*} = (1-\varphi)\beta|\vec{u}_{ai}^{*}|\vec{u}_{ai}^{*} + \varphi|\vec{u}_{io}^{*}|\vec{u}_{io}^{*}. \quad (18)$$

Here we have combined equations (6a) and (6b) to relate the atmosphere-ice and atmosphere-ocean stress velocities via $\vec{u}_{ai}^{*}/\sqrt{C_{ai}} = \vec{u}_{ao}^{*}/\sqrt{C_{ao}}$. Equations (17–18) may in principle be solved analytically following a procedure similar to that described in Sec. 2.2.1: by defining stress velocity components parallel and perpendicular to the atmospheric velocity, $u_{io}^{*\parallel}$, $u_{io}^{*\perp}$, $u_{o}^{*\parallel}$, and $u_{o}^{*\perp}$, analogously to definitions (13a) and (13b). Then taking the dot product of $\vec{u}_{ai}^{*}$ and $\hat{Z} \times \vec{u}_{ai}^{*}$ with each of (17) and (18) yields four scalar equations that can be solved simultaneously for the components of $\vec{u}_{io}^{*}$ and $\vec{u}_{o}^{*}$. Finally, using the definitions $|\vec{u}_{io}^{*}|^2 = \left(u_{io}^{*\parallel}\right)^2 + (u_{io}^{*\perp})^2$ and $|\vec{u}_{o}^{*}|^2 = (u_{o}^{*\parallel})^2 + (u_{o}^{*\perp})^2$ yields a pair of equations that must be solved simultaneously for $|\vec{u}_{io}^{*}|$ and $|\vec{u}_{o}^{*}|$. In practice we simply solve (17–18) numerically using least-squares optimization.

2.3 Physical interpretation

Though equations (14–16) constitute an analytical solution to the mixture layer momentum balance (11), in this form they yield little insight into the wind-driven drift of sea ice. We therefore provide additional formulae for some key quantities describing the ice drift. Moreover, we briefly discuss the similarities and differences between our equations and the equations based on Rossby similarity theory (e.g. McPhee 2008; 2012). We base our discussion around the solution for near-100% sea ice concentration, given in section 2.2.1, because this solution is completely analytical and thus offers more insight.

2.3.1 Ice velocity

For convenience we re-state equation (10a), which relates the shear between the ice and the geostrophic ocean velocity to the ice-ocean stress velocity in the case of close to 100% sea ice cover,

$$\vec{u}_i - \vec{u}_g = \left(\frac{1}{\sqrt{C_{io}}} + \frac{1}{\sqrt{2K_0^{*}}}\right)\vec{u}_{io}^{*} - \frac{1}{\sqrt{2K_0^{*}}}\hat{Z} \times \vec{u}_{io}^{*}.$$

This equation is similar to the one derived by McPhee (2008; 2012) for the case of an unstratified IOBL, because both approaches assume a traditional Ekman layer solution over most of the IOBL. However, there are some notable differences: Instead of assuming that the turbulent transfer of momentum follows a quadratic drag law, McPhee (2008; 2012) utilized the *law of the wall* equation across the ocean-ice boundary layer, leading to a slightly more complicated version of this equation,

$$\vec{u}_i - \vec{u}_g = \left(\frac{1}{\kappa}\log\left(\frac{|\vec{u}_{io}^*|}{f z_0}\right) + \frac{1}{\kappa}\log\left(\frac{K_0^*}{\kappa}\right) + \frac{1}{\sqrt{2K_0^*}}\right)\vec{u}_{io}^* - \frac{1}{\sqrt{2K_0^*}}\hat{Z} \times \vec{u}_{io}^*,$$

where κ is Karman's constant ($\kappa = 0.4$) and z_0 is hydraulic roughness at the bottom of sea ice. Because the velocity profile over the ocean-ice boundary layer is assumed to be logarithmic (i.e. following the *law of the wall*), logarithmic terms appear as coefficients of ice-ocean stress velocity $\vec{u}_{io}^*$. In our equation (10a) these terms are replaced by $1/\sqrt{C_{io}}$, due to our assumption of a linear relationship between the ice-ocean shear and the ice-ocean stress velocity.

Our formulation is arguably a less accurate description of the IOBL when the sea ice concentration is close to 100% because it does not allow the ice speed to vary nonlinearly with the ice-ocean stress velocity. However, in general the sea ice concentration may be much smaller than 100%, and at any given horizontal location the surface boundary condition is transient, varying between a solid upper boundary (the ice) and a free surface (open water). Thus the assumption of a flow following the *law of the wall* and the notion of a hydraulic roughness length no longer applies to this case. We have therefore assumed quadratic drag laws at these interfaces for simplicity, but in principle a more accurate IOBL model could be derived following the ideas of Rossby similarity theory but using a transient surface boundary condition that varies between a solid boundary and a free surface.

2.3.2 Turning angles

The IOBL turning angle is the angle between the ice-ocean stress velocity $\vec{u}_{io}^*$ and the ice-geostrophic shear $(\vec{u}_i - \vec{u}_g)$, and may be defined as

$$\cos(\theta_{IOBL}) = \frac{\vec{u}_{io}^{*} \cdot (\vec{u}_i - \vec{u}_g)}{|\vec{u}_{io}^{*}||\vec{u}_i - \vec{u}_g|}. \quad (\text{~~17~~}19)$$

ThusIn our model, the IOBL turning angle for near-100% sea ice concentration is

$$\cos(\theta_{IOBL}) = \frac{1+\alpha}{\sqrt{1+(1+\alpha)^2}}, \quad (20)$$

which is independent of the surface wind speed ~~for 100% sea ice concentration. Equations (5)~~ and ~~(6c),~~depends only on the parameter $\alpha = \sqrt{2K_0^*/C_{io}}$. Thus for near-100% sea ice concentration, prescribing an Ekman spiral and a linear relationship between the ice–ocean stress velocity $\vec{u}_{io}^{*}$ and the ice–ocean shear ~~($\vec{u}_i$~~($\vec{u}_i - \vec{u}_o$~~), are~~) is equivalent to assuming a constant geostrophic ice-ocean turning angle (e.g. Hibler, 1979; Thorndike and Colony, 1982). ~~In reality θ_{IOBL} depends on~~By contrast the ~~ice-ocean stress $\vec{u}_{io}^{*}$, but the~~IOBL turning angle predicted by Rossby similarity theory varies ~~by only~~as a function of the ice-ocean stress velocity, and the turning angle varies by a few degrees over a realistic range of ice–ocean stress magnitudes (McPhee, 1979; 2008).

Note that in our model θ_{IOBL} is generally not independent of the surface wind speed when the sea ice concentration is below 100%. Fig. 2 shows the IOBL turning angle θ_{IOBL} as a function of α. The IOBL turning angle θ_{IOBL} decreases from 45 degrees to zero as α increases from zero to infinity. A larger value of α corresponds to a relatively large vertical diffusivity K_0^*, which tends to reduce the magnitude of the shear in the Ekman layer. Thus the shear becomes dominated by the surface boundary layer, over which the shear does not turn with depth. A smaller value of α corresponds to a relatively large drag coefficient C_{io}, which tends to reduce magnitude of the shear in the surface boundary layer. Thus the shear becomes dominated by the Ekman spiral, over which the shear turns by 45 degrees. This is consistent with Rossby similarity theory (McPhee 2008; 2012) in that multi-year ice pack with a relatively high basal hydraulic roughness corresponds to a larger a larger turning angle θ_{IOBL}. In this study, we employ the canonical value of K_o^* = 0.028 (McPhee, 1994; 2008), and we use C_{io}=0.0071 based on the estimate of Cole et al. (2014) from the ITP-V data. This combination of K_o^* and C_{io} produces a θ_{IOBL} of around 15 degrees (red dot in Fig. 2). This value is within the

range of turning angles predicted by Rossby similarity theory, which is about 20 degrees for multi-year ice pack and 13 degrees for the first-year ice (McPhee 2012).

We now turn to the ice drift itself. We derive the angle between the 10m wind speed $\vec{u}_a$ and the ice-geostrophic shear $\vec{u}_i - \vec{u}_g$ by taking the dot product of $\vec{u}^*_{ai}$ with (10a), noting that $\vec{u}^*_{ai}$ lies parallel to $\vec{u}_a$ from (6a), and using (14) and (15) for the components of $\vec{u}^*_{io}$,

$$\cos(\theta_{ai}) = \frac{k_o|\vec{u}^*_{io}|^2}{k_a|\vec{u}^*_{ai}|^2}\frac{1+\alpha}{\sqrt{1+(1+\alpha)^2}} = \frac{|\vec{\tau}_{io}|}{|\vec{\tau}_{ai}|}\cos(\theta_{IOBL}) \qquad (\text{~~18~~}21)$$

Using equation (16) above, it is straightforward to show that the ratio of the ice–ocean to air–ice stresses is smaller than one, $k_o|\vec{u}^*_{io}|^2/k_a|\vec{u}^*_{ai}|^2 = |\vec{\tau}_{io}|/|\vec{\tau}_{ai}| < 1$, so it follows that the air–ice angle is always at least as large as the IOBL turning angle, $\theta_{ai} \geq \theta_{IOBL}$. This reflects the fact that the 10-m wind velocity $\vec{u}_a$ always points to the left of the ice–ocean stress $\vec{\tau}_{io}$ (*c.f.* equations (14) and (15)), while the ice–geostrophic shear $\vec{u}_i - \vec{u}_g$ always points to the right of $\vec{\tau}_{io}$ (*c.f.* equation (10a)). For strong winds ($|\vec{\tau}_{ai}| \to \infty$) equation (16) implies that the air–ice and ice–ocean stresses balance one another in (3) (i.e. $\vec{\tau}_{io} \to \vec{\tau}_{ai}$), so the air-ice turning angle becomes independent of the wind speed and equal to the IOBL turning angle. For weak winds ($|\vec{\tau}_{ai}| \to 0$) equation (16) implies that the ice–ocean to air–ice stress ratio vanishes, $|\vec{\tau}_{io}|/|\vec{\tau}_{ai}| \to 0$[1], so from (18) the ice velocity becomes directed 90° to the right of the winds.

3 Observation and Reanalysis Datasets

In this section we detail the various observational and reanalysis datasets used to ~~validate~~evaluate our analytical model and to quantify how southerly winds affects Arctic

[1] To obtain this result from equation (16), first note that if $|\vec{u}^*_{ai}| = 0$ then the only non-negative real solution to (16) is $|\vec{u}^*_{io}| = 0$, so we can conclude that $|\vec{u}^*_{io}| \to 0$ as $|\vec{u}^*_{ai}| \to 0$. Then note that in the limit of vanishing air-ice stress, $|\vec{u}^*_{ai}| \to 0$, equation (16) can only remain balanced if $|\vec{u}^*_{io}| \sim |\vec{u}^*_{ai}|^2$. It follows that $|\vec{\tau}_{io}|/|\vec{\tau}_{ai}| \to 0$ as $|\vec{u}^*_{ai}| \to 0$.

summer sea- ice concentration.

3.1 Observations

To ~~validate~~evaluate our analytical model with observations, we used observations from an ice-tethered profiler (ITP; Toole et al., 2010) equipped with a velocity sensor (ITP-V; Williams et al., 2010). Specifically, we use data from ITP-V 35, which was deployed on October 8, 2009 on an ice floe in the Beaufort Sea at 77° N, 135° W, as part of the Beaufort Gyre Observing System (BGOS). The ice floe was 2.6 m thick, so hydrostatic adjustment resulted in an ice–ocean interface at around 2.3 m depth (Cole et al. 2014). Ocean velocity profiles were obtained every 4 h to 150 m depth, with an effective vertical resolution of 1 m. To examine the ice–ocean shear $(\vec{u}_i - \vec{u}_o)$ and the ice-ocean velocity angle, we use the shallowest ~~consistently available~~ measurements from the velocity profiles, at a depth of 7 m. The ice velocity $(\vec{u}_i)$ is derived from hourly GPS fixes and linearly interpolated in time to align with the time of the ITP-V 35 observations. Further details, including calibrations and a discussion of errors in ITP-V 35, are described by Cole et al. (2014).

Arctic sea- ice concentration data is from the U.S. National Snow and Ice Data Center (NSIDC), and is based on satellite-derived passive microwave brightness temperature. Specifically, the NASA Team Algorithm (Swift and Cavalieri, 1985) was used to estimate the sea- ice concentration. These data are provided as a daily mean on a polar stereographic grid with 25 x 25 km resolution. We re-gridded this data onto a regular 1.0° x 1.0° grid.

3.2 Reanalysis

Observations of Arctic sea- ice thickness are sparse, so instead we use the coupled Pan-arctic Ice-Ocean Modeling and Assimilation System (PIOMAS; Zhang and Rothrock, 2003) to estimate the basin scale Arctic sea- ice thickness. PIOMAS consists of a 12-category thickness and enthalpy distribution sea ice model coupled with the POP (Parallel Ocean Program) ocean model (Smith et al., 1992). The data is monthly and covers from the year 1978 to 2013. For ~~atmospheric winds,~~the surface wind stress we used 10 m

winds provided by the European Center for Medium-Range Weather Forecasts ERA-Interim reanalysis dataset (Dee et al., 2011). The data is 6 hourly with a horizontal resolution of 1.0° x 1.0°.

4 ~~Analytical~~ Model ~~validation~~evaluation

In this section, we validate our analytical model ~~against the ITP-V 35 observations of sub-sea ice ocean velocity. Specifically, we examine if the modeled wind-ice and ice-ocean velocity angles are consistent with the observation.~~In this section, we evaluate our analytical model against the ITP-V 35 observations of sub-sea ice ocean velocity (Cole et al., 2014). Specifically, we compare the modeled wind-ice and ice-ocean velocity angles against the observed values. As outlined in the introduction, one might not expect the winter Beaufort Sea to serve as a useful test case because the sea ice concentration is typically close to 100%, so the internal stresses neglected in our model may be dynamically significant (Leppäranta, 2005). Additionally, sea ice formation in winter may produce negative buoyancy forcing that induces strong convection and vertically-varying eddy viscosity in the surface mixed layer, inconsistent with our assumption of as uniform vertical viscosity throughout the Ekman layer (McPhee, 2012). However, the ITP-V 35 measurements indicate that the ice was very close to a free drift regime and experienced weak vertical buoyancy fluxes in the surface mixed layer (Cole et al., 2014), so these features of the winter sea ice pack may be less prominent than in previous observations. For a complete picture of the stratification regime in the observed near-surface ocean, see figures 3, 4, 8 and 9 of Cole et al. (2014). For example, the mixed layer depth over the Beaufort Sea is very shallow in October (~15 m) and deepens to 30–40 m in February and March (Fig. 9 of Cole et al. 2014).

4.1 Model parameters

The ITP-V 35 was deployed upon a 2.6 m-thick ice floe, which is much thicker than the mean ice thickness over the western Beaufort Sea. Fig. 1a shows the PIOMAS sea- ice thickness averaged from October 2009 to March 2010. During this time period, sea- ice thickness over the western Beaufort Sea (around 74-78° N, 135-150° W) is around 1.4–

1.6 m. It is therefore likely that ITP-V 35 was mounted on a relatively sturdy floe, whereas ~~much of~~ the surrounding floes were ~~a lot~~ thinner. Sea ice concentration over this region is mostly over 85-90% from October to March (Fig. 1b). The velocity of the mixture layer (see Sec. 2) represents a bulk average over many floes, and similarly the ocean Ekman layer in any given location responds to stresses transmitted by a series of ice floes passing overhead. For the purpose of model ~~validation~~evaluation we therefore take the sea- ice thickness h_i to be 1.5 m, which is appropriate for basin-scale sea- ice momentum balance. ~~For simplicity and for comparison with Rossby similarity theory, we assume 100% sea ice cover ($\varphi = 1$). This is reasonable because the mean sea ice concentration over the western Beaufort Sea is mostly over 85-90% from October to March (Fig. 1b).~~

Observational fits toExtensive measurements of the ice-ocean boundary layer suggest that the annual mean value of the dimensionless vertical eddy diffusivity K_o^* is about 0.028 (McPhee, 1994; 2008). ~~However, our treatment~~Below we also present model predictions using a nominal enhanced value of $K_o^* = 0.1$, which yields improved agreement between the ~~IOBL in Sec. 2~~model and the observations. A possible explanation for this is ~~formally only applicable to neutrally-stratified boundary layers with no surface buoyancy flux. The~~that the ITP-V observations mostly cover winter season (from October to March), when surface buoyancy loss due to sea ice formation ~~enhances~~can enhance the vertical eddy diffusivity by a factor of up to 10 (McPhee and Morison, 2001). ~~Below we therefore test our model using~~ However, it is more likely that internal stresses in the ice impede its motion, so the canonical value of $K_o^* = 0.028$ ~~and an enhanced~~overestimates the ice drift. Thus the reader should not infer from our results that using a larger value of K_o^* ~~= 0.1; the former and the latter values might be suitable for the annual mean and winter respectively.~~ is more physically realistic. Finally, the geostrophic current in the interior of polar oceans, $\vec{u}_g$, is poorly constrained, and we assume that this term is small relative to the surface current. This assumption should be more robust on intraseasonal time scales, as surface winds can strengthen rapidly in a few days, so the resultant surface Ekman velocity is likely to be much larger than the interior geostrophic flow.

For other parameters, we used standard values used in many previous studies: $\rho_a =$

1.35 Kg/m^3, $\rho_i = 910$ Kg/m^3, and $\rho_o = 10001026$ Kg/m^3. The atmospheric drag coefficients C_{ai} and C_{ao} depend on the season, the ice fraction, and the surface roughness (Lüpkes et al., 2012), but for simplicity we use a constant values of $C_{ai} = 1.89 \times 10^{-3}$ and $C_{at}C_{ao} = 1.25 \times 10^{-3}$ (Lüpkes and Birnbaum, 2005). We prescribe the ice-ocean drag coefficient C_{io} based on the findings of Cole et al. (2014,), who found that $C_{io} = 7.1 \times 10^{-3}$ best fit the ITP-V 35 measurements. However, we note that it is difficult to calculate C_{io} accurately from the ITP-V data because measurements of the vertical eddy momentum fluxes were made at a depth of 6 m, a few meters below the ice base.

4.2 Results

Fig. 23 shows the observed ice speed (black line) as a function of the 10 m wind speed. Consistent with Thorndike and Colony (1982), the relationship is linear, except for weak winds (speed less than 2 m/s). For moderately strong winds, sea- ice moves with a speed around 1.5–2% of the surface wind speed. This is consistent with or slightly weaker than an old rule-of-thumb that suggeststhe well-known 2% relationship (Thorndike and Colony, 1982). It may be that sea ice formation, and thus surface buoyancy loss, leads to stronger mixing (larger K_o^*) in the IOBL, which reduces the sea ice speed (see Fig. 2). The internal stresses in the relatively concentrated sea ice (85-90% in winter) may also impede sea ice motion. In general, our 3a shows that the analytical model (red and blue lines) predicts this relationship quite well, though only the solution with strong vertical diffusivity ($K_o^* = 0.1$) is within the error bars. As introduced, ITP-V 35 was deployed mostly during winter, so larger vertical diffusivity (blue-dotted line; $K_o^* = 0.1$) fits better with the observation. Using the with the canonical value of K_o^* ($K_o^* = 0.028$) overestimates the observed ice speed by 20–40%, whereas a larger vertical diffusivity (blue-dotted line; $K_o^* = 0.1$) fits better with the observations. As stated above, this is probably because the internal stresses in the relatively concentrated sea ice (85–100% in winter) impede the ice drift. We also compare the observed ice drift speeds with those predicted by 'classical' fee drift (Leppäranta, 2005), in which we neglect both the Ekman layer velocity and the geostrophic velocity. Mathematically this corresponds to assuming

an infinitely large vertical diffusivity ($K_o^* \to \infty$) in our model. This classical free drift (blue solid line in Fig. 3a) is about 30-~~50%.~~% slower than the ice drift with an interactive Ekman layer (red line in Fig. 3a), verifying that the IOBL substantially enhances the wind-induced ice speed.

Fig. 3b shows that there is little difference in ice speed between 100% sea ice cover (red line; $\varphi = 1$) and 50% sea ice cover (red line; $\varphi = 1$) in this model (Fig. 3b). As shown in equation (10a), the ice-ocean drag coefficient, C_{io}, also directly influences the wind-induced ice velocity. The bottom panels of Fig. 3 show the sensitivity of the ice speed to C_{io} for $K_o^* = 0.1$ (Fig. 3c) and $K_o^* = 0.028$ (Fig. 3d) respectively. Decreasing C_{io} from 0.0071 to 0.004 increases ice speed up to 20–25%. In the Appendix we calculate C_{io} using the ITP-V data and plotted C_{io} both as a function of 10 m wind speed and surface stress (Fig. A1). Consistent with Cole et al. (2014), the individual observed values of C_{io} vary widely, by a factor 10. In general, there is no obvious dependence of C_{io} on the surface stress, so we use the constant value $C_{io} = 0.0071$ of Cole et al. (2014).

Fig. 4~~Fig. 3a~~ shows that the wind–ice velocity angle θ_{ai} decreases as the surface wind strengthens, consistent with previous observations (Thorndike and Colony, 1982). ~~The analytical model with $K_o^* = 0.1$ reproduces this curve remarkably well.~~ The velocity angle is overestimated by 5–10 degrees in the case when the canonical vertical diffusivity $K_o^* = 0.028$ is used (Fig. 4a). The analytical model with $K_o^* = 0.1$ reproduces this curve remarkably well. ~~. From~~Recall from equation (~~18),~~21) that wind-ice velocity angle θ_{ai} ~~is proportional to the ratio between~~ decreases as the ice-ocean to wind-ice stress ratio ($|\vec{\tau}_{io}|/|\vec{\tau}_{ai}|$) increases, and ~~wind-ice stress ($\theta_{ai} \propto |\vec{\tau}_{io}|/|\vec{\tau}_{ai}|$).~~that this stress ratio is always smaller than 1. Thus, the decrease of θ_{ai} with increasing surface wind speed indicates that the stress ratio~~, $|\vec{\tau}_{io}|/|\vec{\tau}_{ai}|$~~ increases as the surface ~~wind strengthens.~~winds strengthen. In other words, the momentum becomes more ~~effectively~~efficiently transferred down to the ocean as the surface wind speed increases. For relatively weak winds, the observational errors in θ_{ai} (gray shadings in Fig. ~~3a) are large, whereas this for stronger winds the air–ice velocity angle is much better constrained (Cole et al., 2014).~~ 4) are large, whereas for stronger winds the air–ice velocity angle is much better constrained (Cole et al., 2014). The wind–ice velocity angle

θ_{ai} estimated using the 'classical' free drift case is about 20 degrees smaller than that predicted by the canonical vertical diffusivity $K_o^* = 0.028$. Moreover, the classical free drift substantially underestimates the observed θ_{ai} even though the internal friction is neglected. This result indicates that the IOBL is essential for properly simulating the direction of the ice drift. Fig. 4b shows that sea ice cover plays a nontrivial role in changing the wind–ice velocity angle θ_{ai}, although the internal stress is neglected in the model. Decreasing sea ice cover from 100% ($\varphi = 1$) to 50% ($\varphi = 0.5$) increases θ_{ai} by 20 degrees for large wind speeds.

The shallowest measurement depth of ITP-V 35 is 7 m, ~~and the~~which is far below the ice base (~2.6 m). The Ekman spiral rotates the velocity ~~quite~~ substantially between the ice base ~~(~2.6 m)~~ and 7 m. Consequently the ITPV data is not suitable for estimating the IOBL turning angle. Instead we test our analytical treatment of the IOBL using the velocity angle between the ice floe and the ocean at 7 m ~~$\theta_{io}|_{z=-7m}$ as a function of ice speed, shown in Fig. 3b. In general, the ice–ocean velocity angle $\theta_{io}|_{z=-7m}$ decreases as ice speed increases.~~, $\theta_{io}|_{z=-7\mathrm{m}}$. ~~Consistent with Cole et al. (2014), the errors in $\theta_{io}|_{z=-7m}$ are quite large, especially for low ice speeds.~~ To calculate $\theta_{io}|_{z=-7\mathrm{m}}$ from the analytical model, the velocity angle needs to be adjusted ~~by~~using the Ekman layer solution, which can be ~~presented~~written as a function ~~of ocean~~ depth, z~~:~~, as

$$\vec{u}(z) = \vec{u}_o \exp\left(\frac{z + h_o}{\delta_E}\right) \exp\left(i\frac{z + h_o}{\delta_E}\right) \qquad (\text{~~19~~})22)$$

Here $\vec{u}_o$ is the ocean surface velocity at the bottom of sea ice, $h_o = (\rho_i/\rho_o)h_i$ is the depth of the ice base, and $\delta_E = \sqrt{2K/f}$ is the Ekman depth. We have used complex variables to describe two-dimensional vectors, *e.g.* $\vec{u}_o = (u_o, v_o) \equiv u_o + iv_o$, because this presents changes in vector orientation more intuitively. The complex term, $\exp(i(z + h_o)/\delta_E)$, produces a velocity $\vec{u}|_{z=-d}$ at any depth d that is rotated relative to $\vec{u}_o$ by a clockwise angle of $(d - h_o)/\delta_E$ radians. Thus the adjusted velocity angle between the ice and the ocean at any depth in the Ekman layer is:

$$\theta_{io}|_{z=-d} = \theta_{io}|_{z=-h_o} + (d - h_o)/\delta_E \qquad (\text{~~20~~})23)$$

In Fig. 5 we plot $\theta_{io}|_{z=-7\mathrm{m}}$ as a function of the ice speed, comparing the predictions of our model with the data from Cole et al. (2014). In general, the ice–ocean velocity angle $\theta_{io}|_{z=-7\mathrm{m}}$ decreases as ice speed increases. Consistent with Cole et al. (2014), the variance in the observationally derived values of $\theta_{io}|_{z=-7\mathrm{m}}$ is quite large, especially for low ice speeds. Our analytical solution for the ice-ocean velocity angle, adjusted using equation (~~20~~23), agrees ~~well~~ reasonably well with the ITP-V 35 measurements. Again, the analytical model predicts the observational curve better when the higher vertical diffusivity of $K_o^* = 0.1$ is used. ~~In summary, the analytical model estimates the observed wind–ice and ice–ocean velocity angles well: for $K_o^* = 0.1$ the model prediction almost always lies within the observational eror bars, indicating that the model captures the essential dynamics of the wind-induced sea-ice motions.~~ Fig. 5b shows that ice concentration is certainly a factor affecting the ice-ocean velocity angle, θ_{io}. Decreasing sea ice cover from 100% to 50% causes a decrease in θ_{io} because the direction of ice drift is constrained by the wind stress over open water between the ice floes ($\vec{\tau}_{ao}$) and the associated surface Ekman transport.

4.3 Parameter sensitivity

~~Having evaluated~~ our ~~analytically tractable solution provides several merits in calculating sea-ice motions. First, this~~ model ~~derives equations~~against the ITP-V 35 measurements using the best available estimates for the ~~mixture of sea ice and water ($\varphi \ll 1$), which is suitable for marginal ice zone. Second, this~~ model ~~describes sea-ice motion as a function~~parameters, we now explore the sensitivity of the model's predictions to key physical properties of ~~ice~~the sea ice itself, namely its thickness ~~h_i.~~and concentration. In Fig. ~~4~~6 we plot the sensitivity of the wind-ice velocity angle (θ_{ai}) and the IOBL turning angle (θ_{IOBL}) to a range of sea- ice concentrations (φ) and ice thicknesses (h_i). In general, the wind-ice velocity angle increases substantially with sea ice thickness (Fig. ~~4a~~6a): for a moderate wind speed of 6 m/s, increasing the sea ice thickness from 0.25 m to 3 m increases this angle from 20° to 60°. ~~By contrast, for 100% sea-ice concentration the IOBL turning angle is independent of the ice thickness (Fig. 4c).~~ It can therefore be inferred from equation (~~18~~)21) and Fig. 6a that thicker ice has smaller stress ratio

$|\vec{\tau}_{io}|/|\vec{\tau}_{ai}|$, implying that thicker ice is less efficient in transferring the momentum into the ocean, leading to larger wind-ice velocity angle~~;~~. In other words, thicker ice absorbs more of the wind-input momentum into the Coriolis torque, transmitting less to the ocean below.

Sea- ice concentration also strongly influences these angles. Consistent with Fig. 4b, Fig. 6b shows that wind-ice velocity angle increases as sea- ice concentration decreases. There is little difference in this angle between 100% and 75% ice concentrations – the angle is less sensitive to relatively high sea- ice concentration. However, the angle rapidly increases as sea- ice concentration gets below 50%: at 25% sea ice concentration the wind-ice angle is 20° larger than at 100% concentration, even for the strongest winds in the dataset. The response of the IOBL turning angle to the mixture of sea ice and water ($\varphi \ll 1$) is rather surprising (Fig. ~~4d~~6d). The turning angle is negative for weaker surface winds in the case when sea- ice concentration is less than 100%. This is because wind stress over the ice-free component of the mixture layer is transmitted directly to the water below. As the sea ice concentration approaches zero, the stress transmitted through the ice becomes negligible in determining the direction of the surface Ekman velocity ($\vec{u}_o$). Because the ITP-V 35 track covers mostly ice-covered regions ($\varphi \approx 1$) and the shallowest measurement depth is 7 m, it is difficult to verify whether negative IOBL turning angles appear in the observations.

5 Application to wind-driven summer sea ice changes

In this section, we quantify the effect of intra-seasonal southerly ~~winds~~wind strengthening events on Arctic sea ice cover using near-surface wind data, and compare the results with satellite observations. There are several notable Arctic weather perturbations in the spring and summer over the Pacific sector of the Arctic Ocean, such as the development of the Arctic dipole mode (Wu et al., 2006), quasi-stationary cyclonic winds (Serreze et al., 2003) and synoptic cyclones (Zhang et al., 2013). These perturbations are often accompanied by rapid strengthening of southerlies and a reduction of the sea ice concentration (SIC) on intraseasonal time scales. In the Arctic summer, sea-

ice thickness is mostly below 2 m (Fig. ~~5a~~7a) and the area of the marginal ice zone with a moderate SIC (25–75%) is quite large (Fig. ~~5b~~7b). We therefore hypothesize that the strengthening of southerlies should efficiently redistribute the sea-ice cover in the summer.

This analysis simultaneously serves as an additional evaluation of our analytical model described in Sec. 2. Our model is particularly appropriate to motions in the marginal ice zone, where internal stress is negligible, and to short-duration intensification of the southerly winds, during which the surface ocean velocity will typically be large compared to the geostrophic velocity. This evaluation could in principle be extended to compare the modeled sea ice velocities directly against sea ice drift products. However, we have chosen to retain our focus on the sea ice concentration rather than the ice drift velocity. Ice drift products exhibit considerable uncertainty, particularly during summer when the ice is typically thinner (Sumata et al., 2014). Furthermore, there is considerable variance in the ice speed and the wind-ice velocity angle even in the ITP-V data (see Figs. 3 and 4), in which the ice velocities are measured accurately using GPS fixes.

5.1 Methods

For surface wind forcing, we used the ERA-Interim reanalysis. Arctic sea-ice concentration data is from the U.S. National Snow and Ice Data Center (NSIDC). The Arctic sea-ice concentration shows multi-decadal declining trend and this trend was removed for each calendar day and for each grid. For sea-ice thickness, we used the climatological mean PIOMAS sea-ice thickness data averaged from 1990 to 2012.

Using the analytical solutions derived in Sec. 2, sea-ice velocity is calculated from the ERA-Interim daily 10-m winds. Then, lagged composite analyses are performed in order to investigate how a rapid development of southerlies affects sea-ice concentration during the Arctic summer. We used data from 1990 to 2012 and focused on the summer, from August 1 to September 30 (AS). To define the events of the rapid strengthening of southerlies, the surface winds over the Pacific sector of the Arctic are zonally and meridionally averaged, from 150°E to 230°E and from 70°N to 90°N (cosine weighting is applied to each latitude). Then, the southerly wind event is defined as a time period when

the averaged southerly wind value exceeds 1 standard deviation for three or more consecutive days. If the beginning of an event occurs within 7 days of the end of the preceding event, then the latter event is discarded. This procedure identifies 27 events during the analysis period. Lag zero is defined as the day when the averaged southerly winds peak. Prior to generating the composites, a 3-day moving average is applied to filter out noise associated with day-to-day fluctuations.

These southerly wind-induced sea-_ice drifts redistribute sea-_ice concentration. This effect is computed using the following evolution equation: ~~d~~$dI_c = -\left[\frac{\partial(U_i I_c)}{\partial x} + \frac{\partial(V_i I_c)}{\partial y}\right]$~~Δt.~~dt. Here I_c is sea-_ice concentration, which ranges from 0 to 1, at each grid point, and ~~Δt~~dt is a time step, which has a length of one day in this study. To calculate sea ice concentration anomalies we subtract the long-term climatological mean ~~d~~dI_c from the daily ~~d~~dI_c during the southerly wind events. Then, the anomalous daily ~~d~~dI_c is integrated from the lag day -8 to estimate the cumulative changes in sea-_ice concentration associated with the southerly wind events:

~~$\Delta I_c = -\sum_{t=-8}^{t=lag}\left[\frac{\partial(U_i I_c)}{\partial x} + \frac{\partial(V_i I_c)}{\partial y}\right]'$ Δt (16)~~

$$\Delta I_c = -\sum_{t=-8}^{t=lag}(dI_c)'dt - \sum_{t=-8}^{t=lag}\left[\frac{\partial(U_i I_c)}{\partial x} + \frac{\partial(V_i I_c)}{\partial y}\right]' dt \qquad (24)$$

Here, prime $(\,)'$ denotes a deviation from the long-term climatological mean. The time integration starts from the lag –8 because the southerly wind events, on average, start about a week before they peak. The results we present are not very sensitive to the starting date. The maximum and the minimum values of the cumulative changes in sea-ice concentration (ΔI_c) are limited by the mean sea-_ice concentration, which ranges between 0% and 100%. For example, if the cumulative changes in the mean sea-_ice concentration ($\Delta I_c + \overline{I_c}$), where $\overline{I_c}$ is the climatological-mean sea-_ice concentration, exceeds 100%, then ΔI_c is given as $(100 - \overline{I_c})$ %. All of the analytical model results presented here use ~~a dimensionless vertical of $K_o^* = 0.028$ (McPhee,~~ the canonical value of vertical diffusivity ($K_o^* = 0.028$) and the ice-ocean drag coefficient of

$C_{io} = 0.0071$ (Cole et al. 2014). As shown in Fig. 3, the wind-induced ice speed is sensitive to both K_o^* and C_{io}.~~2011).~~

5.2 Results

Fig. ~~6~~8 illustrates the response of the SIC (shadings in the left column) to the development of southerlies (vectors in the left column) from the East Siberian and Chukchi Sea. Over a 10~~-~~ day period since the development of southerlies, the SIC in these regions decreases by 7–8%. The relative timing suggests that the reduction of SIC is caused by the southerly wind-induced sea~~-ice drift.~~ ice drift. In the meantime, because of cross-polar flow, SIC on the Atlantic sector slightly increases (blue color). To further test this possibility, the wind-induced redistribution of SIC is calculated using our model, specifically equations (~~A1a–b; see *appendix*).~~17–18). The result, shown in the right column of Fig. ~~1~~8, captures the spatial pattern in the observed SIC anomalies. The anomalous sea~~-~~ ice velocity (vectors in the right column) is generally directed towards the Beaufort Sea, a little east of the surface wind velocity with the drift angle ~~raging~~ranging between 20° and 45°. The calculated SIC anomalies at day +6 (bottom row of Fig. ~~6~~8) are largely consistent with the satellite observed SIC anomalies. However, the calculated SIC anomalies somewhat underestimate the observation. At day +6, the calculated reduction of SIC over the Pacific sector is about ~~4–~~5–6%, whereas the observed reduction of SIC is up to 6~~–7%.~~ 8%. The increase in SIC over the Atlantic sector associated with cross-polar flow is also slightly underestimated.

There are several ~~factors affecting~~possible explanations for the discrepancy between the modeled and observed sea ice concentration anomalies. Over the Atlantic sector, the cross-polar flow increases SIC and the internal stress is likely to increase as well. As mentioned earlier, our ~~calculations.~~analytical model neglect internal stress that can decelerate ice drift and pile up sea ice over the Atlantic sector. It is possible that the real sea~~-~~ ice thickness in the Arctic summer is thinner than the PIOMAS sea~~-~~ ice thickness. While PIOMAS simulates the Arctic sea ice thickness within a reasonable range, the model is known to generally *overestimate the thickness* of measured sea ice thinner than 2 m (Johnson et al. 2012; Schweiger et al. 2011). Or, the vertical diffusivity K_o^* in

August and September might be smaller than 0.028 due to surface buoyancy input resulting from sea ice melt (McPhee and Morison, 2001). The formation of a summer freshwater layer at the ice base can also reduce the ice-ocean drag coefficient C_{io} (Randelhoff et al., 2014), as can changes shape of the ice base. Additionally, the atmosphere-ice drag coefficient may be larger during the summer season due to additional form stress associated with the formation of leads and melt ponds (Lüpkes et al., 2012).

Finally, we ask: to what extent does the IOBL ~~modulate~~accelerate the ~~sea-~~wind-induced ice ~~velocity?~~drift? We have neglected the ocean surface geostrophic velocity in our analytical model calculations, retaining only the surface Ekman layer. However, if the Ekman layer velocity were sufficiently weak compared to the ice velocity then we could simply neglect the ocean velocity altogether. ~~In Fig. 7 we compare the sea ice speed anomalies~~As introduced in Sec. 4, the 'classical' fee drift (zero Ekman layer velocity) corresponds mathematically to the limit of infinitely large vertical diffusivity ($K_o^* \to \infty$) in our model. In Fig. 9 we compare the anomalous sea ice speed associated with the wind-induced ice drift with and without an IOBL included in the model. Both curves have been generated by averaging the sea ice speed anomalies over the Pacific sector of the Arctic (from 150°E to 230°E and from 70°N to 90°N), and then calculating lagged composites across all southerly wind events. ~~This~~Consistent with Fig. 3a, this plot illustrates that the IOBL enhances the wind-induced sea- ice speed ~~by~~ up to 40-50%. We therefore conclude that ~~acceleration of the sea ice speed by~~ the IOBL plays a substantial role in the rapid reduction of SIC associated with strong southerly wind events.

6 Summary and discussion

In this study we have derived an analytical model for wind-induced sea- ice drift~~, validated~~ and evaluated our model against measurements from a velocity sensor-equipped ice-tethered profiler (ITP-V~~), and~~). We then used the model to demonstrate that Arctic southerly wind events can drive substantial reductions in sea ice concentration over short timescales.

Our model ~~is conceptually similar to~~has elements in common with Rossby similarity theory (McPhee, 2008) for the ice–ocean boundary layer (IOBL~~).~~), but differs crucially in the respect that it allows for an arbitrary mixture of ice and open water. The key features of this model are:

1. The ice floes and leads containing open water are described via a bulk "mixture layer", momentum balance, following Gray and Morland (1994).
2. The IOBL consists of an Ekman layer whose depth is assumed to depend linearly on the surface stress velocity (McPhee, 2011), most appropriate for a neutrally stratified IOBL with no surface buoyancy flux (McPhee and Morison, 2001).
3. The transfer of momentum between the 10 m winds, the ice and ocean components of the mixture layer, and the ocean surface layer are assumed to follow a quadratic drag laws. By contrast Rossby similarity theory assumes the 'law of wall' to hold in a narrow boundary layer at the top of the IOBL (McPhee, 2008).

Though the simplicity of our model carries several caveats, discussed below, it also confers several advantages. ~~For example~~As mentioned in the introduction, the analytical tractability of the model makes it very efficient, certainly much more so than running a ~~full~~fully coupled model of the Arctic. This makes the model straightforward to interpret; the analytical expressions in Sec. 2 yield physical insight into the velocity observations from ITP-V 35 and the sea ice concentration data from NSIDC. The model's "mixture layer" formulation (Gray and Morland, 1994) also makes it suitable for the marginal ice zone.

Our analytical approach was possible because we assumed a constant vertical diffusivity in the surface Ekman layer. This simplification results in an IOBL turning angle (θ_{IOBL}) that is independent of ice–ocean stress $\vec{u}_{io}^{*}$ in our model, whereas the turning angle slightly decreases as the ice–ocean stress strengthens in observations (McPhee 2008). It ~~would~~may be ~~straightforward~~possible to extend our model to incorporate Rossby similarity theory and a stratified IOBL, ~~assuming that some means of parameterizing~~but for sea ice concentrations below 100% the surface ~~buoyancy flux were~~

~~available.~~boundary condition must be modified to account for the presence of patches of open water between the ice floes. Importantly, we also neglected internal stresses in the ice, which can feature prominently in the momentum balance when the sea ice concentration is close to 100% (Leppäranta, 2005). ~~Nonetheless,~~

Our analytical model qualitatively reproduces the wind~~-~~-induced ice speed and wind-ice~~-ocean~~ velocity angles ~~predicted by our analytical model match well with~~ in the ~~recent~~ ITP-V 35 observations. ~~This~~The agreement ~~improves if we use a larger IOBL~~ is improved by replacing the canonical value $K_o^* = 0.028$ of the vertical eddy diffusivity~~, which we speculate is either~~ with an enhanced value of $K_o^* = 0.1$. However, this finding should not be interpreted to mean that the enhanced diffusivity is more physically relevant; while the discrepancy between the model and observations may be due to stronger turbulent mixing due to surface buoyancy loss, ~~or~~it is more likely due to impedance of the sea~~-~~ ice motion by internal stress.

~~We applied our~~ analytical model to investigate the strong southerly events in the Arctic summer to estimate the wind-induced reduction of SIC. The calculated reduction of SIC is largely consistent with satellite observations~~, although the reduction rate is somewhat underestimated.~~. Our results verify that the southerly wind-induced sea~~-~~ ice drift can substantially decrease SIC ~~in~~over the course of a week. Because the wind-induced sea~~-~~ ice drift can be directly calculated from our analytical solution, the underlying processes for the sea~~-~~ ice variability might be better identified by utilizing reanalysis data. We suggest that our analytical model can be a flexible tool for identifying and quantifying the mechanisms for the Arctic and Antarctic sea~~-~~ ice cover variability, which is often associated with the changes in the global-scale circulation pattern (Lee et al. 2011; Holland and Kwok 2012; Bitz and Polvani 2012; Li et al. 2014; Wettstein and Deser 2014; Raphael and Hobbs 2014; Park et al. 2015).

Acknowledgements

H.S.P. would like to thank Drs. S. Lee, S.-W. Son, Y. Kosaka and S. Feldstein for helpful

comments and discussions. The authors thank two anonymous reviewers for detailed comments that were particularly helpful for improving the manuscript. H.S.P. was supported by the Basic Research Project of the Korea Institute of Geoscience and Mineral Resources (KIGAM) funded by the Ministry of Knowledge Economy of Korea. A.L.S. was supported by the University of California, Los Angeles, USA. The authors thank John Toole and Sylvia Cole for assistance with the ITP-V 35 observational dataset.

Appendix

In this appendix we discuss the solution of our model, described in Sec. 2.1, for sea ice concentrations below 100% (~~$\varphi \leq 1$~~). In this appendix we calculate the ice-ocean drag coefficient, C_{io}, using the ITP-V data. The ITP-V was programed to record turbulent fluctuations at 6 m depth for 40 minutes on a daily basis. As noted by Cole et al. (2014), C_{io} can be estimated by the relationship between ice-ocean velocity shear and turbulent momentum flux:

$$\sqrt{\overline{u'w'}^2 + \overline{v'w'}^2} = \rho_o C_{io}[(u_i - u_6)^2 + (v_i - v_6)^2]. \quad \text{(A1)}$$

Here the overbar $\overline{(\,)}$ denotes a 40-minute time average and the primes $(\,)'$ denote deviations from the time mean. The ice and 6 m ocean velocities are denoted as $(u_i,\ v_i)$ and $(u_6,\ v_6)$ respectively. Using equation (A1), we calculated daily C_{io} from the ITP-V data, following Cole et al. (2014). In Fig. A1 we plot C_{io} as a function of the surface wind speed and the surface stress.

We begin by simplifying the coefficients in equations (8) and (9) by defining ~~α, k_a, and k_o as in Sec. 2.1, and additionally defining $\beta = \rho_a C_{ao}/\rho_o C_{ai}$;~~

~~$$\alpha\hat{Z} \times \vec{u}^*_{io} + \hat{Z} \times \vec{u}^*_o + \vec{u}^*_o = \varphi k_a |\vec{u}^*_{ai}| \vec{u}^*_{ai} - \varphi k_o |\vec{u}^*_{io}| \vec{u}^*_{io},$$~~ ~~(A1a)~~

~~$$|\vec{u}^*_o| \vec{u}^*_o = (1-\varphi)\beta |\vec{u}^*_{ai}| \vec{u}^*_{ai} + \varphi |\vec{u}^*_{io}| \vec{u}^*_{io}.$$~~ ~~(A1b)~~

~~Here we have combined equations (6a) and (6b) to relate the atmosphere-ice and atmosphere-ocean stress velocities via $\vec{u}^*_{ai}/\sqrt{C_{ai}} = \vec{u}^*_{ao}/\sqrt{C_{ao}}$. Equations (A1a, b) may~~

~~in principle be solved analytically following a procedure similar to that described in Sec. 2.2: by defining stress-velocity components parallel and perpendicular to the atmospheric velocity, $u_{io}^{*\parallel}$, $u_{io}^{*\perp}$, $u_{a}^{*\parallel}$, and $u_{a}^{*\perp}$, analogously to definitions (13a) and (13b). Then taking the dot product of $\vec{u}_{ai}^{*}$ and $\hat{z}\times\vec{u}_{ai}^{*}$ with each of (A1a) and (A1b) yields four scalar equations that can be solved simultaneously for the components of $\vec{u}_{io}^{*}$ and $\vec{u}_{a}^{*}$. Finally, using the definitions $|\vec{u}_{io}^{*}|^2 = (u_{io}^{*\parallel})^2 + (u_{io}^{*\perp})^2$ and $|\vec{u}_{a}^{*}|^2 = (u_{a}^{*\parallel})^2 + (u_{a}^{*\perp})^2$ yields a pair of equations that must be solved simultaneously for $|\vec{u}_{io}^{*}|$ and $|\vec{u}_{a}^{*}|$. In practice we simply solve (A1a–b) numerically using least-squares optimization.~~

References

Bitz, C. M., Fyfe, J., and Flato, G.: Sea ice response to wind forcing from AMIP models, *J. Climate*, **15**, 522–536, 2002.

Bitz, C.M. and Polvani, L. M.: Antarctic Climate Response to Stratospheric Ozone Depletion in a Fine Resolution Ocean Climate Model. *Geophys. Res. Lett.*, **39**, L20705, 2012.

Cole, S. T., Timmermans, M-L., Toole, J. M., Krishfield, R. A., and Thwaites, F. T.: Ekman Veering, Internal Waves, and Turbulence Observed under Arctic Sea Ice, *J. Phys. Oceanogr.*, **44**, 1306–1328, 2014.

Dee, D. P. *et al.*: The ERA-Interim reanalysis: Configuration and performance of the data assimilation system. *Quart. J. Roy. Meteorol. Soc*. **137**, 553–597, 2011.

Gray, J. M. N. T. and Morland, L. W.: A two-dimensional model for the dynamics of sea ice. *Phil. Trans. R. Soc. Lond. A*, **347**, 219–290, 1994.

Hibler, W. D. III.: A dynamic thermodynamic sea ice model. *J. Phys. Oceanogr.*, **9**, 815–846, 1979.

Heorton, D. B. S., Feltham, D. L., and Hunt, J. C. R.: The Response of the Sea Ice Edge to Atmospheric and Oceanic Jet Formation, *J. Phys. Oceanogr.*, **44**, 2292–2316, 2014.

Holland, P. R. and Kwok, R.: Wind-driven trends in Antarctic sea- ice drift, *Nature Geosci*. **5,** 872–875, 2012.

Johnson, M., Proshutinsky, A. et al.: Evaluation of Arctic sea ice thickness simulated by Arctic Ocean Model Intercomparison Project models, *J. Geophys. Res*., **117**, C00D13, doi:10.1029/2011JC007257, 2012.

Kawakuchi, Y. and Mitsudera, H.: A numerical study of ice-drift divergence by cyclonic wind with a Lagrangian ice model. *Tellus*, **60A**, 789–802, 2008.

Lee, S., Gong, T. T., Johnson, N. C., Feldstein, S. B., and Pollard, D.: On the possible link between tropical convection and the Northern Hemisphere Arctic surface air temperature change between 1958-2001. *J. Clim*. **24**, 4350–4367, 2011.

Leppäranta, M.: The Drift of Sea Ice, Springer-Verlag, Berlin, 2005.

Li, X., Holland, D. M., Gerber, E. P., and Yoo, C.: Impacts of the north and tropical Atlantic Ocean on the Antarctic Peninsula and sea ice. *Nature*, **505**, 538–542, 2014.

Liptak, J. and Strong, C.: The winter atmospheric response to sea ice anomalies in the Barents Sea, *J. Clim*., **27**, 914–924, ~~2013~~2014.

Lüpkes, C. and Birnbaum, G.: Surface drag in the Arctic marginal sea- ice zone: a comparison of different parameterisation concepts. *Boundary-Layer. Meteor*., **117**, 179–211, 2005.

Lüpkes, C., Gryanik, V. M., Hartmann, J., and Andreas, E. L.: A parametrization, based on sea ice morphology, of the neutral atmospheric drag coefficients for weather prediction and climate models, *J Geophys. Res.*, **117,** D13, 2012.

McPhee, M. G.: The effect of the oceanic boundary layer on the mean drift of pack ice: Application of a simple model. *J. Phys. Oceanogr*., **9**, 388–400, 1979.

McPhee, M. G.: An analytic similarity theory for the planetary boundary layer stabilized

by surface buoyancy. *Boundary-Layer Meterol*., **21**, 325–339, 1981.

McPhee, M. G.: On the turbulent mixing length in the oceanic boundary layer. *J. Phys. Oceanogr*. **24**, 2014–2031, 1994.

McPhee, M. G. and Morison, J. H.: Under-ice boundary layer. *Encyclopedia of Ocean Sciences*, 3069–3076, Elsevier, 2001.

McPhee, M. G.: *Air-ice-ocean interaction: turbulent ocean boundary layer exchange processes*, Springer, chapters 4 and 9, 2008.

McPhee, M. G.: Advances in understanding ice–ocean stress during and since AIDJEX, *Cold Reg. Sci. Technol.*, **76**, 24–36, 2012.

Ogi, M. and Wallace, J. M.: The role of summer surface wind anomalies in the summer Arctic sea ice extent in 2010 and 2011, *Geophys. Res. Lett*., **39**, L09704, 2012.

Park, H.-S., Lee, S., Son, S.-W., Feldstein, S. B. and Kosaka, Y.: The impact of poleward moisture and sensible heat flux on Arctic winter sea ice variability, *Journal of Climate*, **28,** 5030-5040, 2015.

Pedlosky, J.: *Geophysical Fluid Dynamics* (second edition), Springer-Verlag, pp. 227–232, 1987.

Plueddemann, A. J., Krishfield, R., Takizawa, T., Hatakeyama, K., and Honjo, S.: Upper ocean velocities in the Beaufort Gyre. *Geophys. Res. Lett.*, **25**, 183–186, 1998.

Raphael, M. N. and Hobbs, W.: The influence of the large-scale atmospheric circulation on Antarctic sea ice during ice advance and retreat seasons, *Geophys. Res. Lett*., 10.1002/2014GL060365, 2014.

Randelhoff, A. and Sundfjord, A. and Renner, A. H. H.: Effects of a Shallow Pycnocline and Surface Meltwater on Sea Ice--Ocean Drag and Turbulent Heat Flux. *Journal of Physical Oceanogr*., **44**, 2176-2190, 2014.

Schweiger, A., Lindsay, R., Zhang J., Steele M., Stern, H., and Kwok, R.: Uncertainty in modeled Arctic sea ice volume, *J. Geophys. Res.*, **116**, C00D06, doi:10.1029/2011JC007084, 2011.

Serreze, M. C., Maslanik, J. A., Scambos, T. A., Fetterer, F., Stroeve, J., and co-authors.: A record minimum arctic sea ice extent and area in 2002. *Geophys. Res. Lett.*, **30**, 1110, 2003.

Smith, R. D., Dukowicz, J. K., and Malone, R. C.: Parallel ocean general circulation modeling, *Phys. D.*, **60**, 38–61, 1992.

Sorteberg, A. and Kvingedal, B.: Atmospheric forcing on the Barents Sea winter ice extent, *J. Clim.*, **19**, 4772–4784, 2006.

Sumata, H., T. Lavergne, F. Girard-Ardhuin, N. Kimura, M. A. Tschudi, F. Kauker, M. Karcher, and R. Gerdes.: An intercomparison of Arctic ice drift products to deduce uncertainty estimates, *J. Geophys. Res. Oceans*, **119**, 4887–4921, (2014).

Swift, C. T. and Cavalieri, D. J.: Passive microwave remote sensing for sea ice research. *Trans. AGU* **66**, 1210–1212, 1985.

Thorndike, A. S. and Colony, R.: Sea ice motion in response to geostrophic winds. *J. Geophys. Res.* **87**, 5845–5852, 1982.

Toole, J. M., Timmermans, M.-L., Perovich, D. K., Krishfield, R. A., Proshutinsky, A., and Richter-Menge, J. A.: Influences of the ocean surface mixed layer and thermohaline stratification on Arctic sea ice in the central Canada Basin. *J. Geophys. Res.*, **115**, C10018, doi:10.1029/2009JC005660, 2010.

Uotila, P., O'Farrell, S., Marsland, S. J., and Bi, D.: A sea- ice sensitivity study with a global ocean-ice model. *Ocean Modelling*, **51**, 1–18, 2012.

Wettstein J. J. and Deser, C.: Internal Variability in Projections of Twenty-First-Century Arctic Sea Ice Loss: Role of the Large-Scale Atmospheric Circulation. *J. Clim*, **27**, 527–

550, 2014.

Williams, A. J., Thwaites, F. T., Morrison, A. T., Toole, J. M., and Krishfield, R.: Motion tracking in an acoustic point-measurement current meter. *Proc. OCEANS 2010 IEEE*, Sydney, Australia, IEEE, 1–8, doi:10.1109/OCEANSSYD.2010.5603862., 2010.

Wu, B., Wang, J., and Walsh, J. E.: Dipole anomaly in the winter Arctic atmosphere and its association with sea ice motion, *J. Clim*, **19**, 210–225, 2006.

Zhang, J., and Rothrock, D. A.: Modeling global sea ice with a thickness and enthalpy distribution model in generalized curvilinear coordinates, *Mon. Weather Rev.*, **131**, 681–697, 2003.

Figure ~~Legends~~Captions

Figure 1: **(a)** sea- ice thickness (m) and **(b)** sea- ice concentration (%), averaged from October 2009 to March 2010. Sea- ice thickness is from PIOMAS and sea- ice concentration data is from NSDIC.

Figure 2: Sensitivity of the IOBL turning angle (θ_{IOBL}) to α ($= \sqrt{2K_0^*/C_{io}}$), calculated from equation (20). The red dot corresponds to the canonical value for the vertical eddy diffusivity (K_o^* =0.028) and blue dot corresponds to a nominal enhanced value (K_o^* = 0.1).

Figure 3: Sensitivity of ice speed (~~m~~cm/s) to 10 m wind speed (m/s). The black line shows the mean value calculated from ITP-V 35 observations binned by 10 m wind speed, and the gray shadings indicate the range of one standard deviation from the mean. The red-, dotted blue and solid blue lines correspond to our analytical model, described in Sec. 2, with **(a)** vertical diffusivities K_o^* = 0.028, 0.1 and ~~0.1~~∞ (no IOBL) respectively. The sensitivity of the ice speed to the ice concentration (φ) is shown in **(b)**; the red and blue lines indicate 100 % ice cover ($\varphi = 1$) and 50% ice cover ($\varphi = 0.5$) respectively. The bottom panel shows the sensitivity of ice speed to ice-ocean drag coefficient (C_{io}), with vertical diffusivities **(c)** K_o^* = 0.028 and **(d)** K_o^* = 0.1 respectively. The bulk sea- ice

thickness is taken to be 1.5 m.

Figure ~~3~~4: The velocity angle (clock-wise rotation angle) ~~**(a)**~~ between the 10 m winds and the ITPV-35 ice floe~~, and **(b)** between the ice floe and the ocean velocity at 7 m depth,~~ as functions of the 10 m wind speed (m/s~~) and ice speed (cm/s) respectively. ~~). Note that typically the ice velocity lies to the right of the wind velocity~~, and the ocean velocity again lies to the right of the ice velocity.~~. In each plot the black line is mean observed value from the ITP-V 35 dataset, binned by wind speed and ice speed respectively, and the gray shadings indicate the range of one standard deviation from the mean. In **(a)**, the red, dotted blue and solid blue lines correspond to our analytical model, described in Sec. 2, with vertical diffusivities K_o^* ~~The~~= 0.028, 0.1 and ∞ (no IOBL) respectively. In **(b)**, the red and blue lines correspond to ~~our analytical model, described~~100% ($\varphi = 1$) and 50% ($\varphi = 0.5$) sea ice concentrations, in ~~Sec. 2, with~~each case using the canonical vertical ~~diffusivities~~diffusivity $K_o^* = 0.028$ ~~and 0.1 respectively~~.

Figure 5: The velocity angle (clock-wise rotation angle) between the ice floe and the ocean velocity at 7 m depth, as functions of the ice speed (cm/s). In each plot the black line is mean observed value from the ITP-V 35 dataset, binned by wind speed and ice speed respectively, and the gray shadings indicate the range of one standard deviation from the mean. In **(a)**, the red and blue lines correspond to our analytical model, described in Sec. 2, with vertical diffusivities K_o^* ~~**Figure 4**: *Analytical model sensitivity to various parameters:*~~ = 0.028 and 0.1 respectively, and using 100 % ice concentration, $\varphi = 1$. In **(b)**, the red and blue lines correspond to 100% ($\varphi = 1$) and 50% ($\varphi = 0.5$) sea ice concentrations, in each case using the canonical vertical diffusivity $K_o^* = 0.028$.

Figure 6: Sensitivity of **(a, b)** wind-ice velocity angle and **(c, d)** IOBL turning angle to various values of **(a, c)** sea- ice thickness h_i (m) and **(b, d)** sea- ice concentration (φ) as a function of 10 m wind speed (abscissa; m/s). In all panels the dimensionless vertical diffusivity is fixed at $K_o^* = 0.028$. In **(a, c)** we use 100% sea ice concentration ($\varphi = 1$), and in **(b, d)** we use a sea ice thickness of $h_i = 1.5$ m.

Figure ~~5~~7: Aug-Sep climatological mean **(a)** sea- ice thickness (m) and **(b)** sea- ice concentration (%) ~~during the years of~~between 1990- and 2012. Sea- ice thickness is from PIOMAS and sea- ice concentration data is from NSDIC.

Figure ~~6~~8: Composites of the anomalous sea- ice concentration (%) calculated from NSIDC satellite observations (left column) and from our analytical model using ERA-Interim ~~10m~~10 m wind velocity data (right column) for lag -2 days (first row), 0 days (second row), 2 day (third row), and lag +6 days (fourth row). See Sec. 5 for a full description of this calculation. Vectors indicate the anomalous 10m winds from reanalysis (m/s; left column) and calculated sea- ice velocity (cm/s; right column). For the anomalous 10m winds (left column) and sea- ice velocity (right column), only vectors stronger than 1.5 m/s and 3.0 cm/s are plotted respectively.

Figure ~~7~~9: Lagged composite of the calculated sea- ice speed (cm/s) associated with the strong southerly events in the presence (red line) and in the absence (black line) of ~~a surface Ekman layer~~an IOBL in our analytical model (in the absence of an Ekman layer the ocean surface velocity is simply set to zero~~).~~ – the classical free drift case). The sea- ice speed is area-averaged over the Pacific sector of the Arctic (from 150°E to 230°E and from 70°N to 90°N). The sea ice speeds that include the surface Ekman layer (red line) identical to those used to construct Fig. ~~6.~~8. The dimensionless vertical diffusivity is set to $K_o^* = 0.028$ and $K_o^* = \infty$ for the IOBL (red line~~).~~) and no-IOBL (black line) cases respectively.

Figure A1: Sensitivity of the ice-ocean drag coefficient C_{io} to **(a)** the surface wind speed (m/s) and **(b)** the surface stress (kg/m/s^2), calculated using equation (A1). The black line shows the mean value calculated from ITP-V 35 observations and the gray shadings indicate the range of one standard deviation from the mean. The red line corresponds to the value estimated by Cole et al. (2014) based on least-squares approximation.

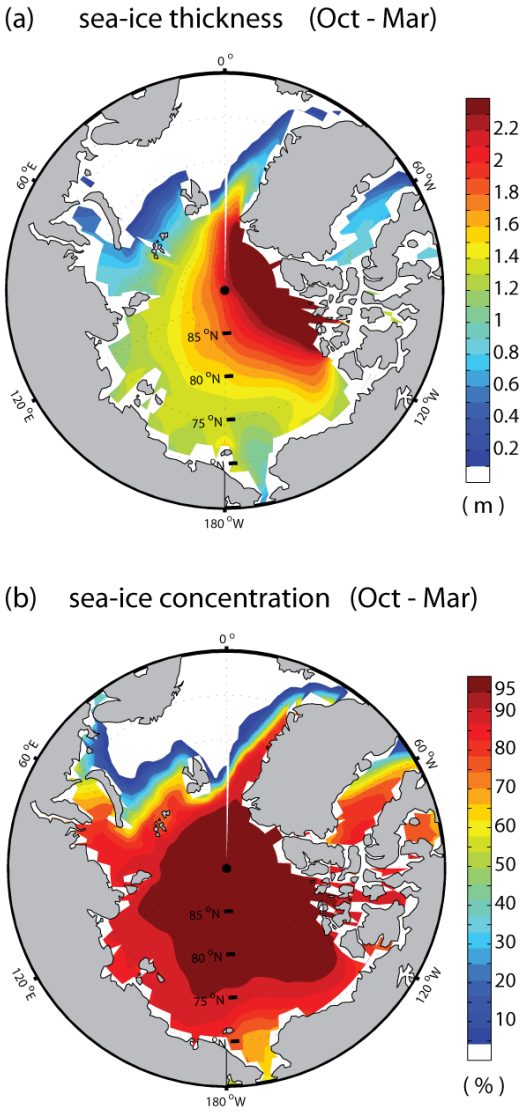

Figure 1: **(a)** sea-ice thickness (m) and **(b)** sea-ice concentration (%), averaged from October 2009 to March 2010. Sea-ice thickness is from PIOMAS and sea-ice concentration data is from NSDIC.

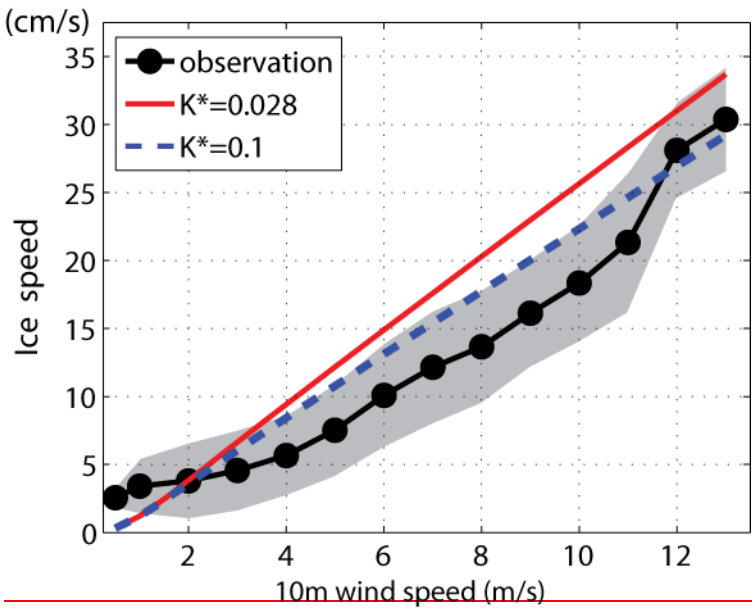

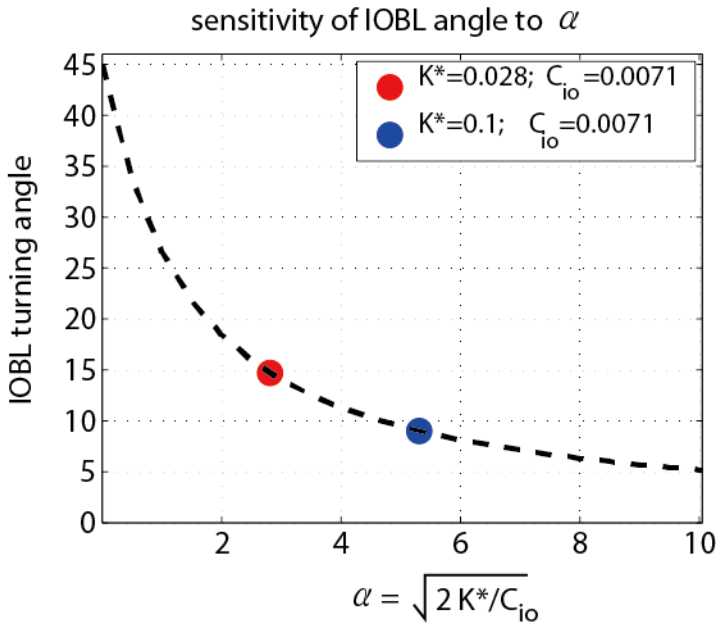

Figure 2: Sensitivity of the IOBL turning angle (θ_{IOBL}) to α (= $\sqrt{2K_0^*/C_{io}}$), calculated from equation (20). The red dot corresponds to the canonical value for the vertical eddy diffusivity (K_o^* =0.028) and blue dot corresponds to a nominal enhanced value (K_o^* = 0.1).

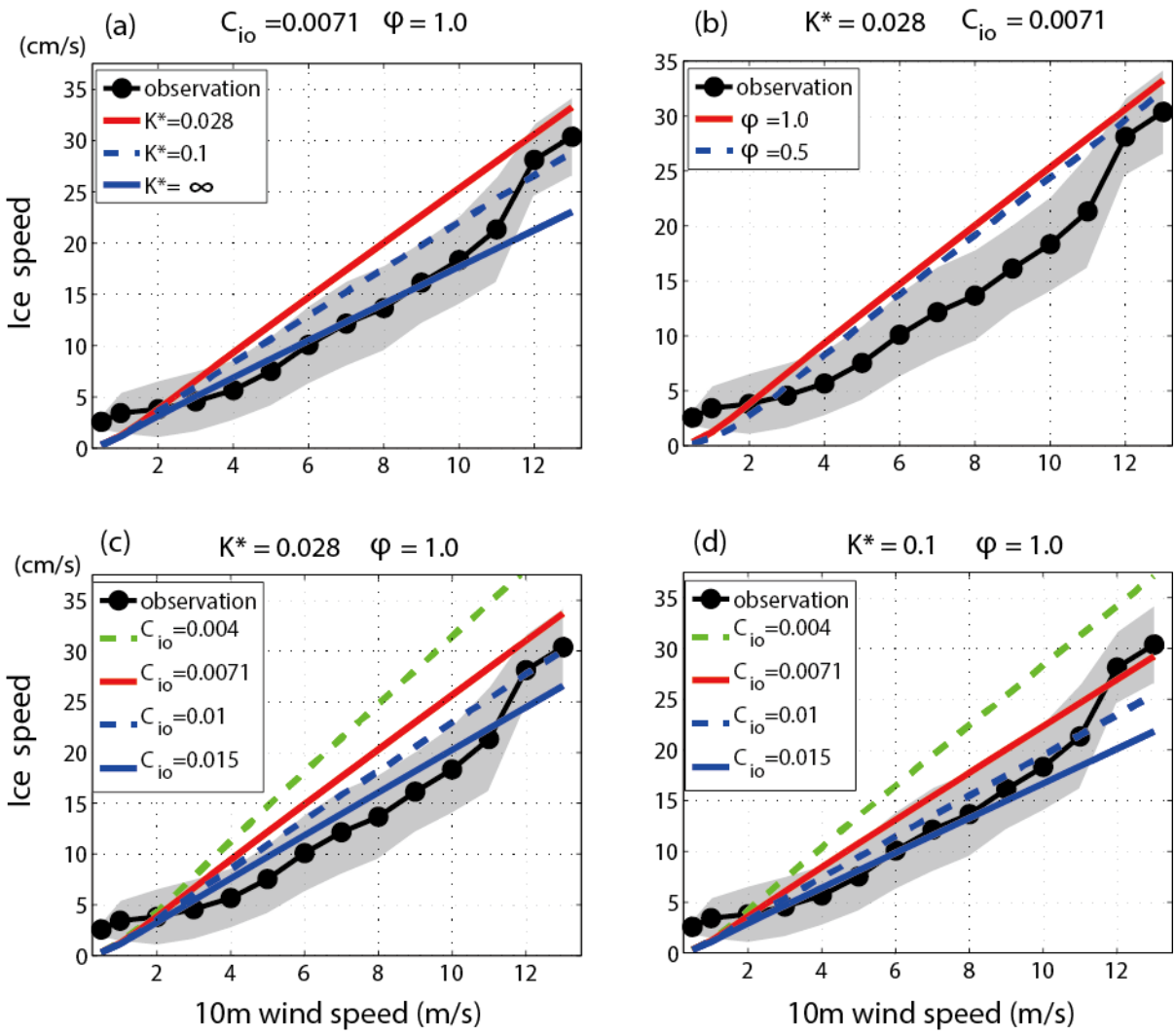

~~Figure~~ 3: Sensitivity of ice speed (~~m~~cm/s) to 10 m wind speed (m/s). The black line shows the mean value calculated from ITP-V 35 observations binned by 10 m wind speed, and the gray shadings indicate the range of one standard deviation from the mean. ~~The red and blue lines correspond to our analytical model, described in Sec. 2, with vertical diffusivities K_o^* = 0.028 and 0.1~~The red, dotted blue and solid blue lines correspond to our analytical model, described in Sec. 2, with **(a)** vertical diffusivities K_o^* = 0.028, 0.1 and ∞ (no IOBL) respectively. The sensitivity of the ice speed to the ice concentration (φ) is shown in **(b)**; the red and blue lines indicate 100 % ice cover (φ = 1) and 50% ice cover (φ = 0.5) respectively. The bottom panel shows the sensitivity of ice speed to ice-ocean drag coefficient (C_{io}), with vertical diffusivities **(c)** K_o^* = 0.028 and **(d)** K_o^* = 0.1

respectively. The bulk sea- ice thickness is taken to be 1.5 m.

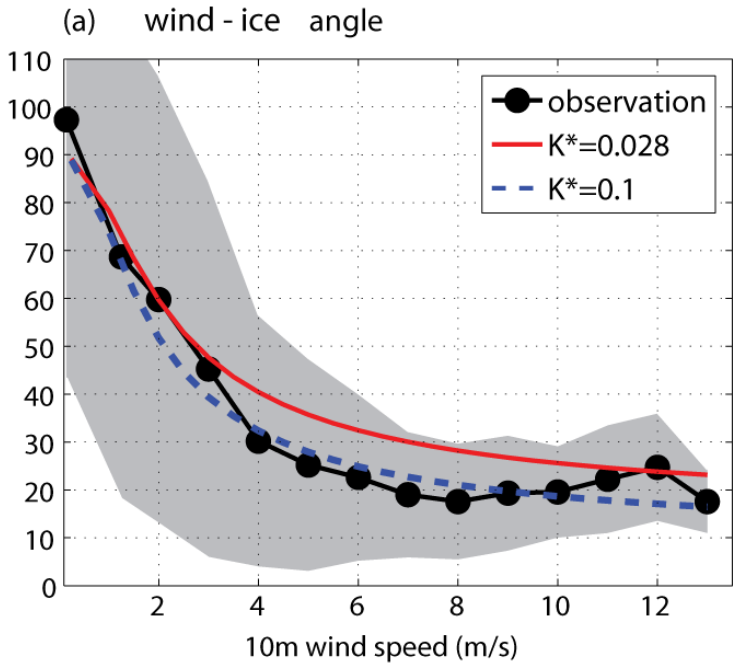

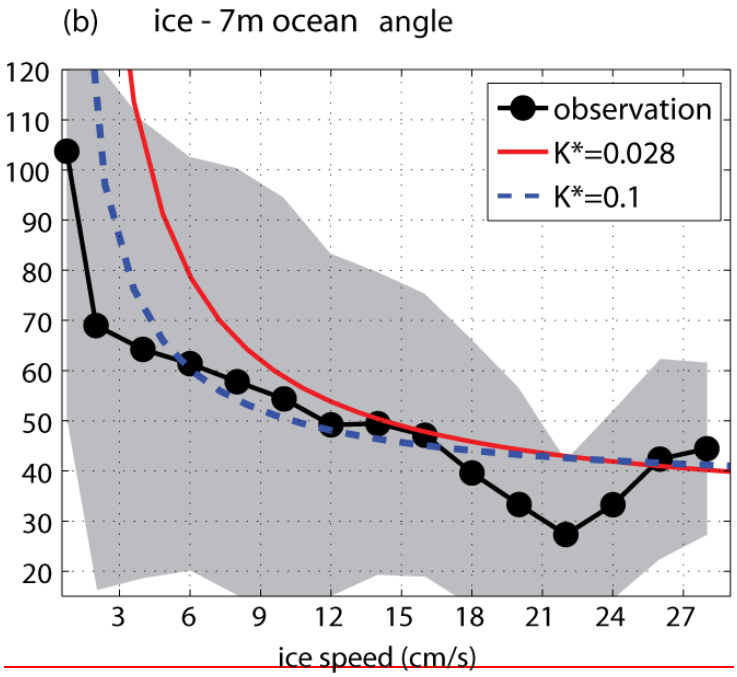

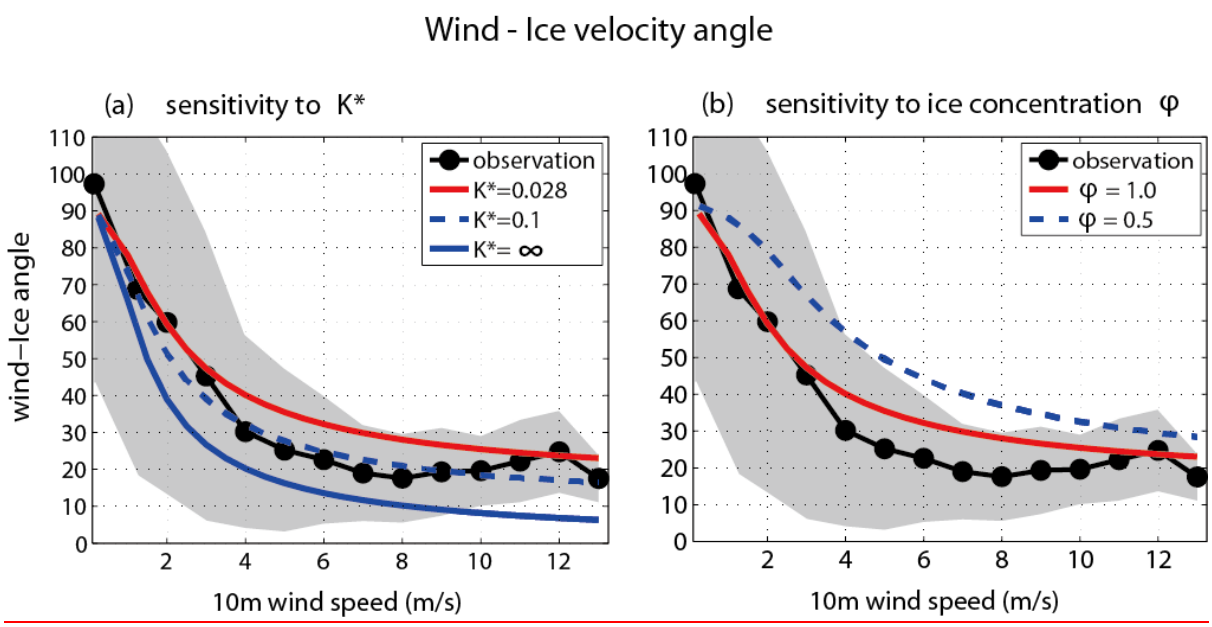

Figure ~~3~~4: The velocity angle (clock-wise rotation angle) ~~**(a)**~~ between the 10 m winds and the ITPV-35 ice floe~~, and **(b**~~ as functions of the 10 m wind speed (m/s). Note that typically the ice velocity lies to the right of the wind velocity. In each plot the black line is mean observed value from the ITP-V 35 dataset, binned by wind speed and ice speed respectively, and the gray shadings indicate the range of one standard deviation from the mean. In **(a)**, the red, dotted blue and solid blue lines correspond to our analytical model, described in Sec. 2, with vertical diffusivities K_o^* = 0.028, 0.1 and ∞ (no IOBL) respectively. In **(b)**, the red and blue lines correspond to 100% ($\varphi = 1$) and 50% ($\varphi = 0.5$) sea ice concentrations, in each case using the canonical vertical diffusivity K_o^* = 0.028.

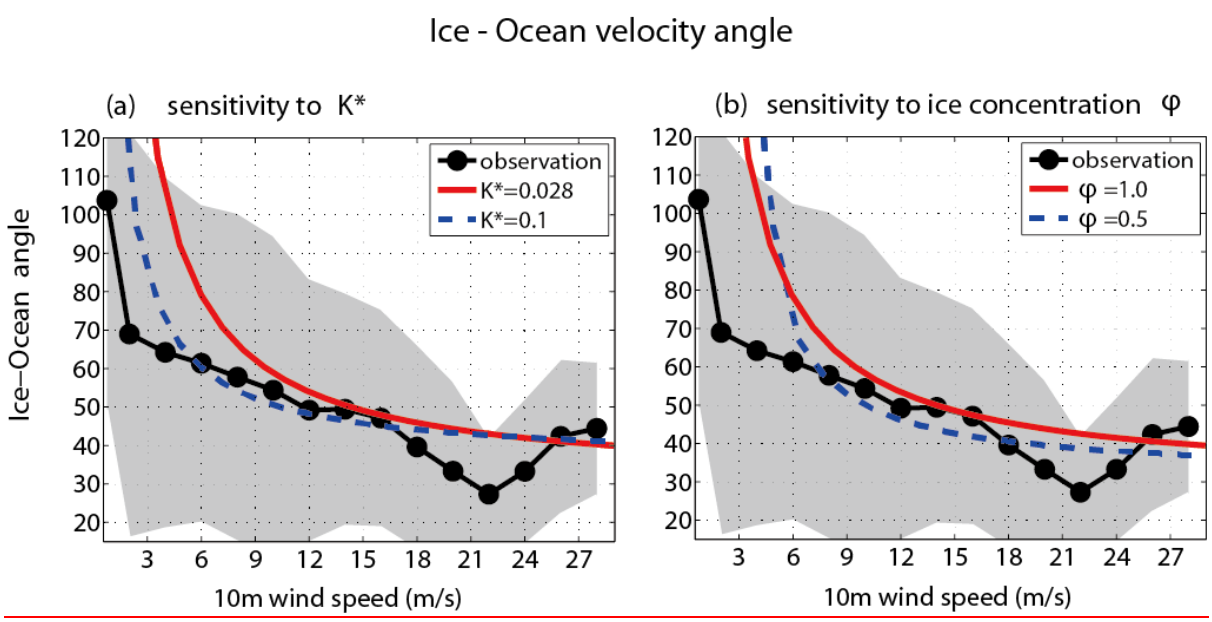

~~**Figure** 5~~: The velocity angle (clock-wise rotation angle) between the ice floe and the ocean velocity at 7 m depth, as functions of the ~~10 m wind speed (m/s) and ice speed (cm/s) respectively. Note that typically the ice velocity lies to the right of the wind velocity, and the ocean velocity again lies to the right of the ice velocity. In each plot the black line is mean observed value from the ITP-V 35 dataset, binned by wind speed and ice speed respectively, and the gray shadings indicate the range of one standard deviation from the mean. The red and blue lines correspond to our analytical model, described in Sec. 2, with vertical diffusivities K_o^* = 0.028 and 0.1 respectively~~ice speed (cm/s). In each plot the black line is mean observed value from the ITP-V 35 dataset, binned by wind speed and ice speed respectively, and the gray shadings indicate the range of one standard deviation from the mean. In **(a)**, the red and blue lines correspond to our analytical model, described in Sec. 2, with vertical diffusivities K_o^* = 0.028 and 0.1 respectively, and using 100 % ice concentration, $\varphi = 1$. In **(b)**, the red and blue lines correspond to 100% ($\varphi = 1$) and 50% ($\varphi = 0.5$) sea ice concentrations, in each case using the canonical vertical diffusivity K_o^* = 0.028.

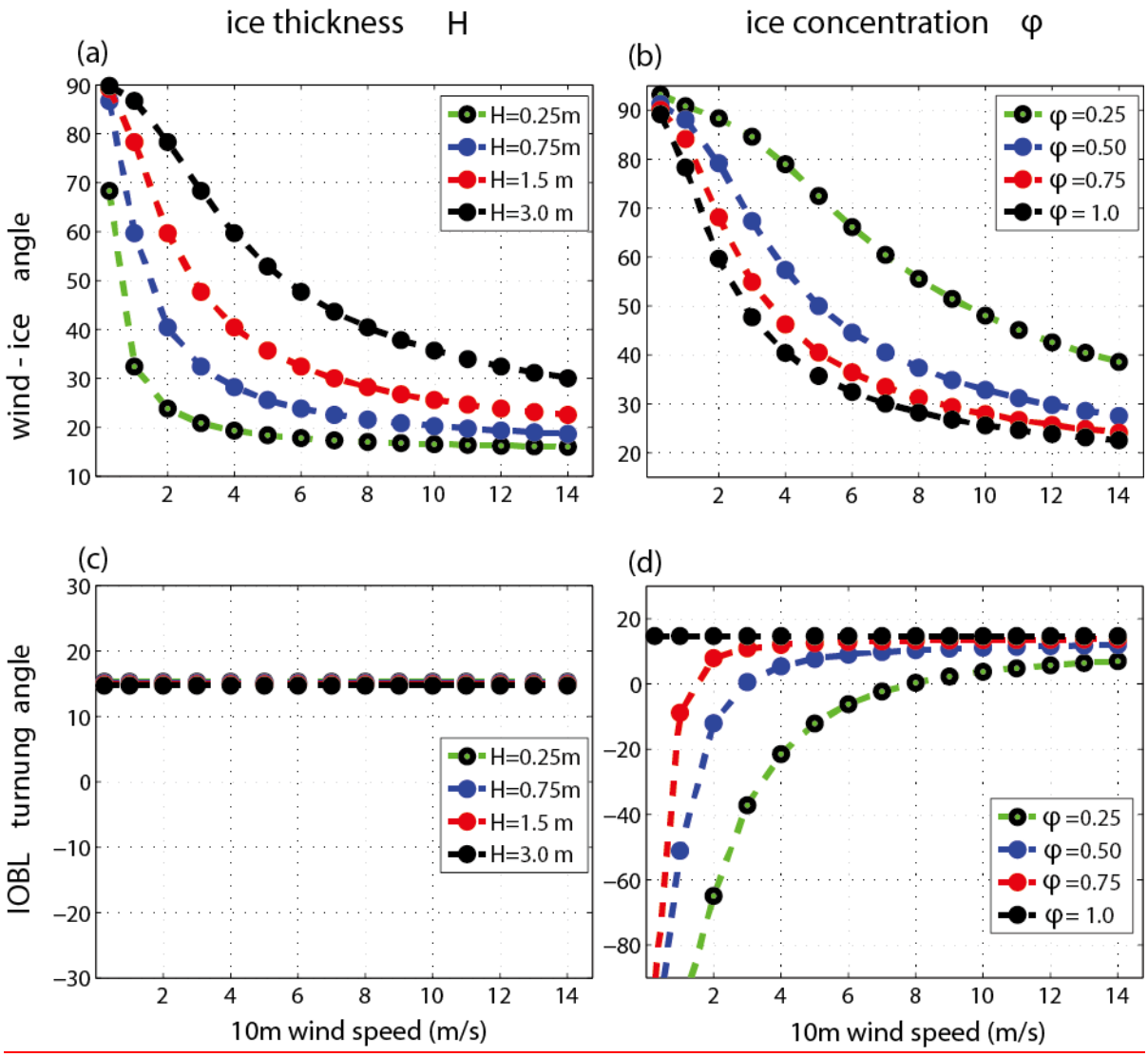

Figure 6: Sensitivity of **(a, b)** wind-ice velocity angle and **(c, d)** IOBL turning angle to various values of **(a, c)** sea-ice thickness h_i (m) and **(b, d)** sea-ice concentration (φ) as a function of 10 m wind speed (abscissa; m/s). In all panels the dimensionless vertical diffusivity is fixed at K_o^* = 0.028. In **(a, c)** we use 100% sea ice concentration ($\varphi = 1$), and in **(b, d)** we use a sea ice thickness of $h_i = 1.5$ m.

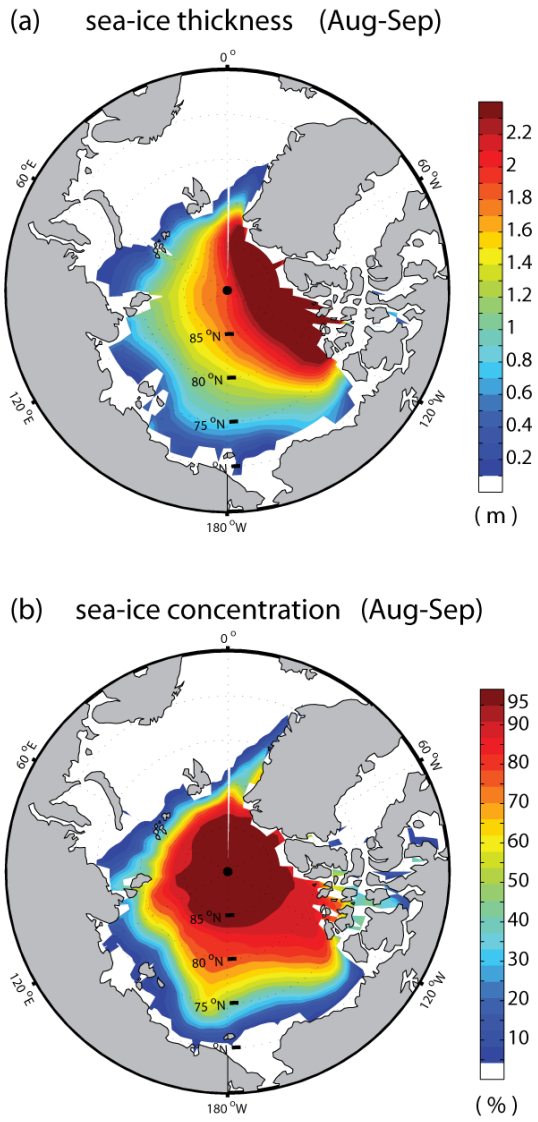

Figure ~~5~~7: Aug-Sep climatological mean **(a)** sea-~~ice~~ ice thickness (m) and **(b)** sea-~~ice~~ ice concentration (%) ~~during the years of~~between 1990-~~ice~~ and 2012. Sea-~~ice~~ ice thickness is from PIOMAS and sea-~~ice~~ ice concentration data is from NSDIC.

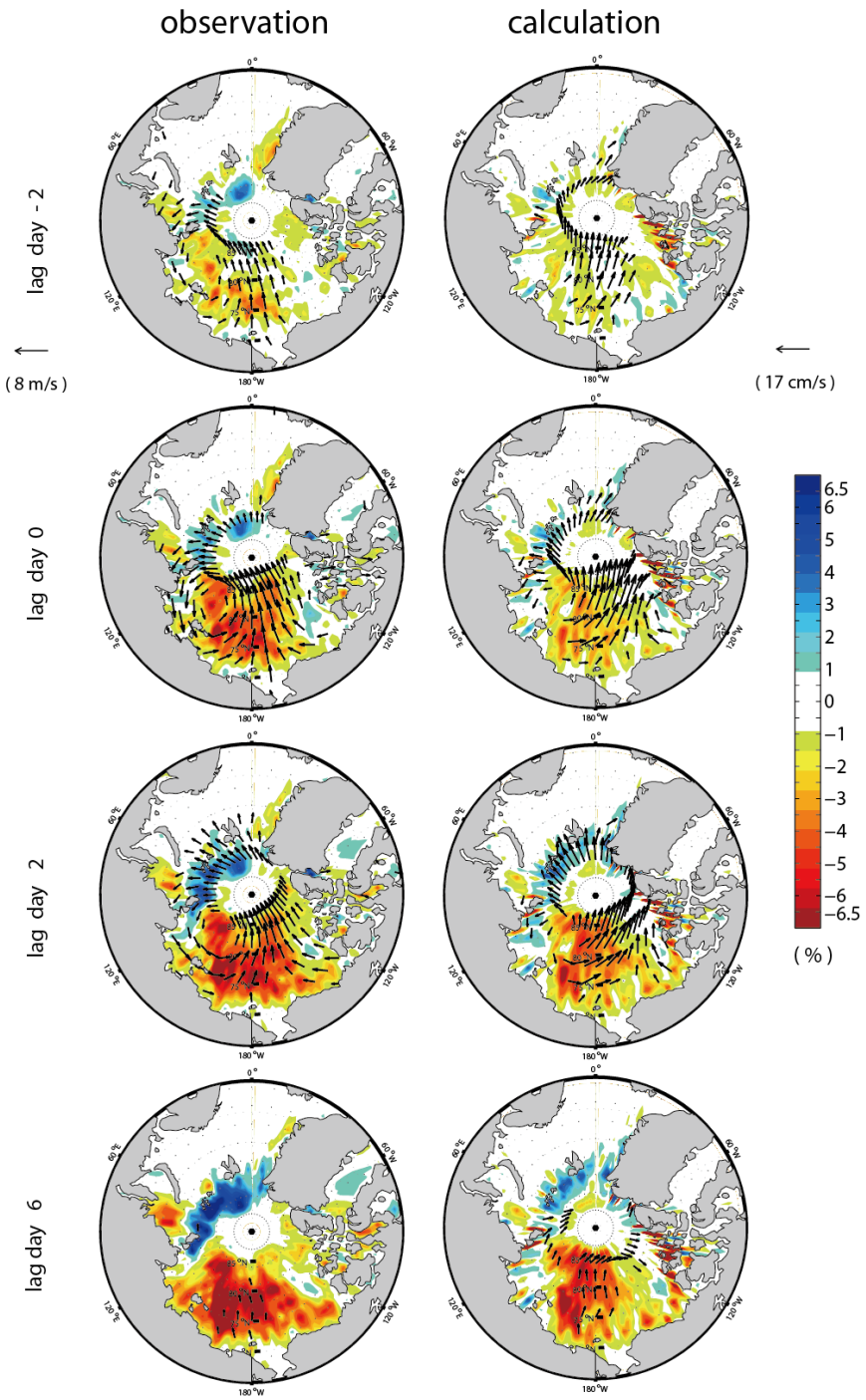

Figure 68: Composites of the anomalous sea-_ice concentration (%) calculated from NSIDC satellite observations (left column) and from our analytical model using ERA-Interim 10 m wind velocity data (right column) for lag -2 days (first row), 0 days (second row), 2 day (third row), and lag +6 days (fourth row). See Sec. 5 for a full description of

this calculation. Vectors indicate the anomalous 10m winds from reanalysis (m/s; left column) and calculated sea- ice velocity (cm/s; right column). For the anomalous 10m winds (left column) and sea- ice velocity (right column), only vectors stronger than 1.5 m/s and 3.0 cm/s are plotted respectively.

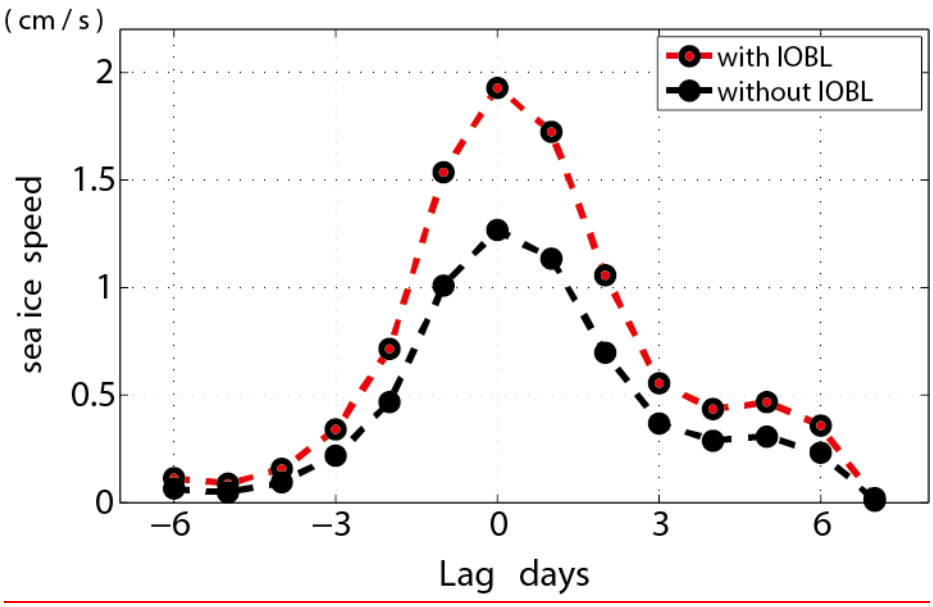

Figure ~~7~~9: Lagged composite of the calculated sea- ice speed (cm/s) associated with the strong southerly events in the presence (red line) and in the absence (black line) of ~~a surface Ekman layer~~an IOBL in our analytical model (in the absence of an Ekman layer the ocean surface velocity is simply set to zero~~).~~ – the classical free drift case). The sea- ice speed is area-averaged over the Pacific sector of the Arctic (from 150°E to 230°E and from 70°N to 90°N). The sea ice speeds that include the surface Ekman layer (red line) identical to those used to construct Fig. ~~6.~~8. The dimensionless vertical diffusivity is set to $K_o^* = 0.028$ and $K_o^* = \infty$ for the IOBL (red line~~).~~) and no-IOBL (black line) cases respectively.

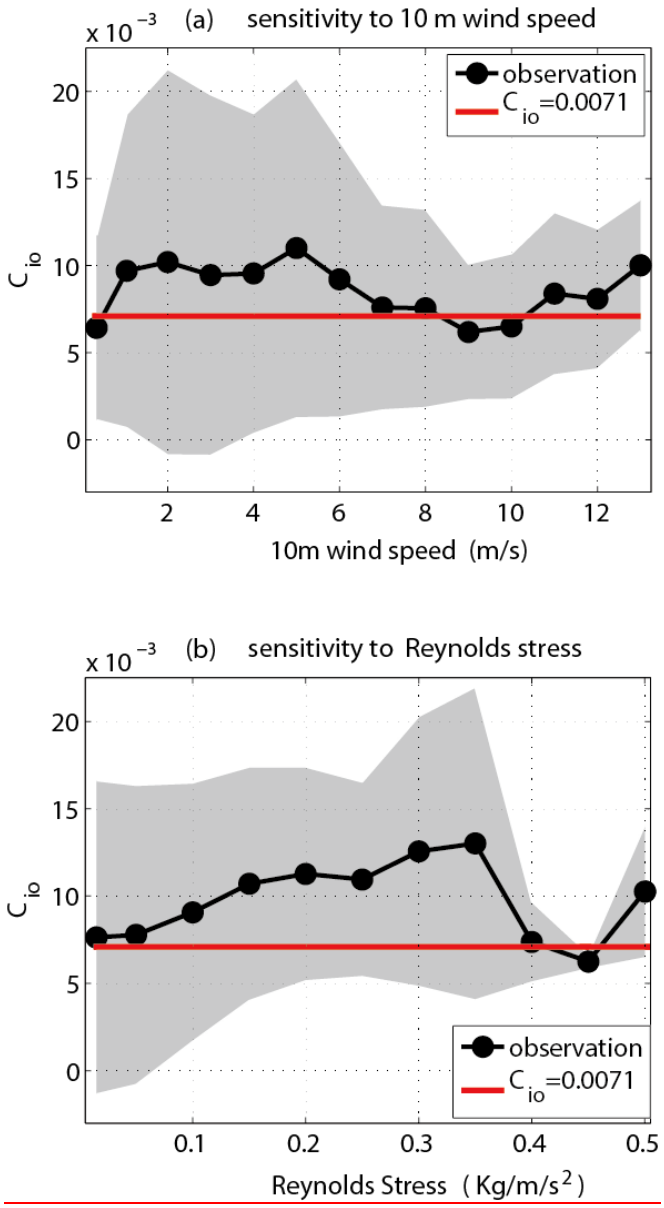

Figure A1: Sensitivity of the ice-ocean drag coefficient C_{io} to **(a)** the surface wind speed (m/s) and **(b)** the surface stress (kg/m/s^2), calculated using equation (A1). The black line shows the mean value calculated from ITP-V 35 observations and the gray shadings indicate the range of one standard deviation from the mean. The red line corresponds to the value estimated by Cole et al. (2014) based on least-squares approximation.